ACS central science

http://pubs.acs.org/journal/acscii

Research Article

Chemical Inhibition of ENL/AF9 YEATS Domains in Acute Leukemia

Leopold Garnar-Wortzel,[▽] Timothy R. Bishop,[▽] Seiya Kitamura,[▽] Natalia Milosevich, Joshua N. Asiaban, Xiaoyu Zhang, Qinheng Zheng, Emily Chen, Anissa R. Ramos, Christopher J. Ackerman, Eric N. Hampton, Arnab K. Chatterjee, Travis S. Young, Mitchell V. Hull, K. Barry Sharpless, Benjamin F. Cravatt, Dennis W. Wolan, and Michael A. Erb*

Cite This: *ACS Cent. Sci.* 2021, 7, 815–830

Read Online

ACCESS | Metrics & More | Article Recommendations | Supporting Information

ABSTRACT: Transcriptional coregulators, which mediate chromatin-dependent transcriptional signaling, represent tractable targets to modulate tumorigenic gene expression programs with small molecules. Genetic loss-of-function studies have recently implicated the transcriptional coactivator, ENL, as a selective requirement for the survival of acute leukemia and highlighted an essential role for its chromatin reader YEATS domain. Motivated by these discoveries, we executed a screen of nearly 300,000 small molecules and identified an amido-imidazopyridine inhibitor of the ENL YEATS domain (IC_{50} = 7 μM). Improvements to the initial screening hit were enabled by adopting and expanding upon a SuFEx-based approach to high-throughput medicinal chemistry, ultimately demonstrating that it is compatible with cell-based drug discovery. Through these efforts, we discovered SR-0813, a potent and selective ENL/AF9 YEATS domain inhibitor (IC_{50} = 25 nM). Armed with this tool and a first-in-class ENL PROTAC, SR-1114, we detailed the biological response of AML cells to pharmacological ENL disruption for the first time. Most notably, we discovered that ENL YEATS inhibition is sufficient to selectively suppress ENL target genes, including *HOXA9/10*, *MYB*, *MYC*, and a number of other leukemia proto-oncogenes. Cumulatively, our study establishes YEATS domain inhibition as a viable approach to disrupt the pathogenic function of ENL in acute leukemia and provides the first thoroughly characterized chemical probe for the ENL YEATS domain.

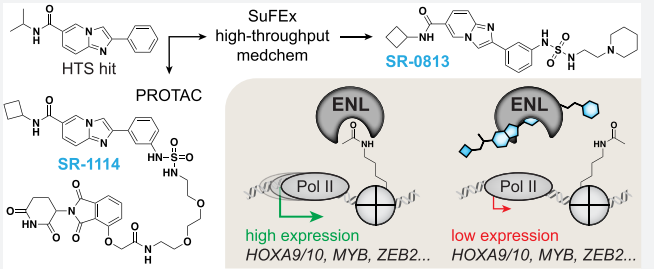

INTRODUCTION

Transcriptional dysregulation in cancer pathogenesis represents a potentially rich source of targets for therapeutic intervention. In acute myeloid leukemia (AML), genetic alterations disproportionately affect transcriptional machinery and frequently converge on similar nodes of pathogenic gene control, like ectopic activation of *HOXA* cluster genes.[1−9] Tragically, despite being the second-most-common leukemia, the 5-year survival rate of patients with AML remains around 25%. Therefore, there is significant interest in drugs and drug targets that would enable the suppression of the core transcriptional circuitries driving AML pathogenesis. Motivated to illuminate such targets, we previously applied genome-scale CRISPR/Cas9 loss-of-function screening to identify genes that are required for AML survival.[10] Through this work, and contemporaneously with others, we identified the transcriptional coactivator ENL (encoded by *MLLT1*) as a requirement for the proliferation of AML and B-ALL (B-cell acute lymphoblastic leukemia) that harbor oncogenic rearrangements of the *multiple lineage leukemia* (MLL) gene.[10,11] MLL rearrangements drive expression of *HOXA* genes, leading to the formation of a particularly aggressive subset of acute leukemia.[12] While these leukemia depend on ENL for survival, normal hematopoietic stem and progenitor cells (HSPCs) do not,[10,11] suggesting a putative therapeutic window for ENL antagonism in MLL-fusion leukemia.

ENL is a chromatin reader protein possessing an amino-terminal YEATS domain (named for the first-discovered members of the family: Yaf9, ENL, AF9, Taf14, Sas5) and a disordered carboxy-terminal protein−protein interaction interface.[13] Adapted to bind acylated lysine side chains, the YEATS domain of ENL is thought to mediate its localization to acetylated regions of chromatin, mainly gene promoters.[10,11] ENL then recruits additional transcriptional effectors, such as the super elongation complex (SEC), that regulate transcription by RNA polymerase (Pol) II.[10,11,14] Presently, the ENL YEATS domain is known to bind with low micromolar affinity to acetyl (ac) and crotonyl (cr) modifications of lysine residues found within the amino-terminal tails of histone

Received: November 17, 2020
Published: April 30, 2021

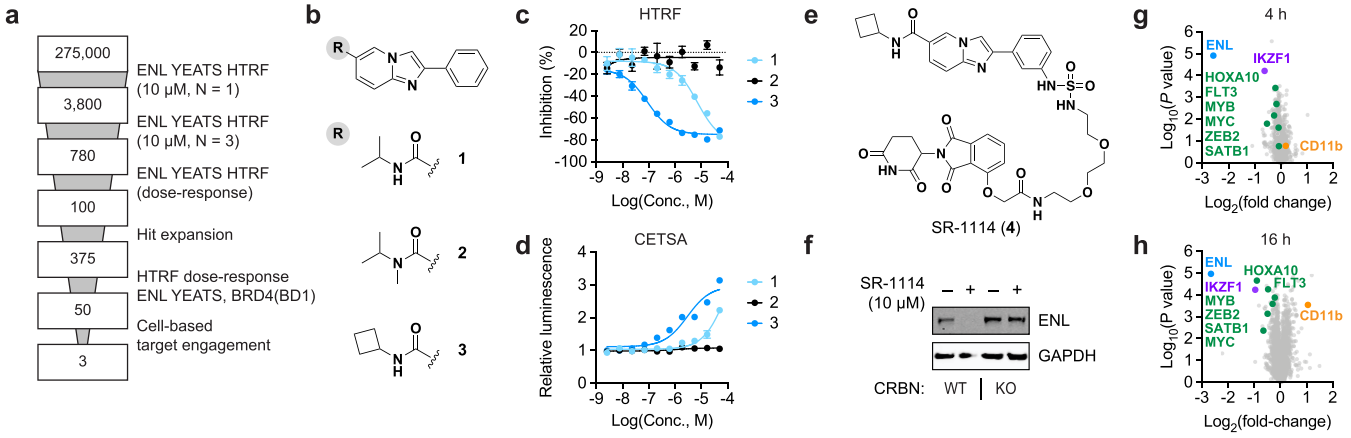

Figure 1. Amido-imidazopyridine scaffold with activity against ENL/AF9 YEATS domains. (a) Summary of screening campaign to identify and validate ligands for the ENL YEATS domain. (b) Structure of screening hit, **1**, and compounds used for preliminary SAR-finding studies. (c) Activity against the ENL YEATS domain measured by HTRF. Mean percent inhibition ± s.e.m., $n = 4$. (d) Engagement of ENL(YEATS)-HiBiT measured by ligand-induced luminescence. Signal normalized to DMSO ± s.e.m., $n = 4$. (e) Chemical structure of SR-1114 (**4**). (f) Immunoblot confirmation of CRBN-dependent ENL degradation by SR-1114. (g, h) Volcano plots depicting DMSO-normalized changes in protein abundance in MV4;11 cells after 4 h (g) and 16 h (h) treatments of SR-1114 (10 μM). Depicted are 6972 proteins with at least 2 unique spectral counts detected. ENL target genes are shown in green. *P* values derived from two-tailed Student's *t*-test, $n = 3$.

H3.[10,11,15] While the post-translational modifications it binds are localized to all gene promoters, ENL is asymmetrically distributed to its genomic binding sites in AML cells.[10] That is, a small number of genes, including a disproportionate number of leukemia proto-oncogenes and dependencies, are occupied with a disproportionate amount of ENL at their promoters. To understand the impact of this asymmetry on ENL-dependent transcriptional control, we previously used degradation tag (dTAG) technology to engineer a tagged ENL allele that is sensitive to pharmacologically induced degradation.[10,16] The rapid kinetics of this system allowed us to probe the direct effects of ENL loss at early time points and revealed that asymmetrically loaded ENL target genes are preferentially sensitive to the loss of ENL. As a result, a number of disease-relevant leukemia drivers, such as *HOXA9/10*, *MEIS1*, *MYB*, and *MYC*, are selectively suppressed by the acute loss of ENL.[10] However, since the dTAG system relies on over-expression of an ENL-FKBP12(F36V) fusion protein, direct-acting chemical tools are needed to confirm these results. Additionally, given the extensive efforts required to engineer the dTAG system in mammalian cell lines, chemical tools would enable a broader study of ENL in diverse model systems.

The YEATS domain represents a compelling target for chemical probe development as genetic experiments have suggested it is (i) required to mediate a stable association of ENL with chromatin and (ii) essential for the proliferation of ENL-dependent leukemia.[10,11] However, it remains unknown if ENL YEATS inhibition is sufficient to recapitulate the transcriptional suppression of ENL target genes observed by ENL-dTAG degradation. Unfortunately, the inhibition of an isolated chromatin reader domain often fails to reproduce the biological effects of disrupting the entire protein by genetic knockouts or knockdowns. This has been observed on multiple occasions for bromodomains, chromatin readers that also bind acetyllysine.[17] For instance, SMARCA2 and SMARCA4 are compelling targets in multiple cancer types,[18−21] but high affinity ligands targeting their bromodomains fail to recapitulate the effects of genetic knockdowns.[22] Ultimately, the inhibition of SMARCA2/4 function requires a different domain to be targeted or the proteins to be degraded entirely.[23−26] The same is true of the bromodomain protein, TRIM24.[27] Therefore, as a final, definitive step in target identification, it is essential to study the biological effects of directly engaging the ENL YEATS domain with small-molecule ligands.

Recent disclosures of small-molecule and synthetic peptide ligands have established the druggability of ENL and AF9 (encoded by *MLLT3*) YEATS domains.[28−33] However, the phenotypes observed in AML cells following genetic suppression of ENL have yet to be validated with direct-acting chemical tools. The most potent small-molecule ENL/AF9 YEATS inhibitor reported to date, SGC-iMLLT (K_d = 129 nM), has not been studied in AML cells beyond proximal measures of target engagement.[29] Importantly, its effects on leukemia survival and ENL-dependent gene expression programs have yet to be described,[31] underscoring the need to not only discover but also fully characterize potent and selective ENL chemical probes. Here, we have undertaken such efforts, reporting on the development and characterization of advanced chemical tools for the ENL YEATS domain.

Through a coordinated effort in discovery chemistry that began with high-throughput chemical screening, we developed an ENL degrader, SR-1114, and ENL YEATS inhibitor, SR-0813. Our discovery of SR-0813 (K_d = 30 nM) relied on a high-throughput medicinal chemistry approach that leverages biocompatible SuFEx transformations to synthesize hit analogs in highly parallel, miniaturized formats. As previously demonstrated, the crude products of these reactions can be tested directly in biochemical assays without further purification, expediting the process of medicinal chemistry.[34] Here, we extend this approach by demonstrating that SuFEx-based high-throughput medicinal chemistry is compatible with cell-based measures of activity, which ultimately proved essential for the identification of SR-0813. By mechanistically and thoroughly studying SR-0813 in AML model systems with integrative transcriptional genomics, we define the impact of ENL inhibition on pathogenic gene control and highlight the remarkably selective suppression of leukemic ENL target genes. Together, these studies provide the first pharmaco-

https://doi.org/10.1021/acscentsci.0c01550
ACS Cent. Sci. 2021, 7, 815−830

logical validation of the ENL YEATS domain as a target in MLL-fusion leukemia and advance a high-quality chemical probe to study ENL/AF9 YEATS domains.

RESULTS

In prior research efforts, we and others used mutational approaches to identify a critical role for the YEATS domain in ENL-dependent leukemia proliferation.[10,11] Interested to validate these results with direct-acting pharmacological tools as well as to investigate the YEATS domain in ENL-dependent transcriptional control, we undertook efforts to discover chromatin-competitive inhibitors of the ENL YEATS domain. Using a homogeneous time-resolved FRET (HTRF)-based measure of binding between the ENL YEATS domain and a histone H3 peptide crotonylated at Lys27 (H3K27cr), we screened for putative ENL YEATS inhibitors from a collection of approximately 275,000 diverse small molecules (Figure 1a). Confirmed primary hits were tested in dose−response format, leading to the selection of 100 compounds for hit-expansion studies and further evaluation. In total, these 100 hits and an additional 275 structurally similar analogs were tested in dose−response assays against ENL YEATS and then counter-screened against the first bromodomain (BD1) of BRD4 (a structurally dissimilar protein fold that also recognizes acetyllysine residues).[17] To validate ENL binding by an orthogonal measure and to prioritize cell-permeable compounds, YEATS-selective hits were evaluated in a luminescence-based cellular thermal shift assay (CETSA) that measures intracellular engagement of an ENL(YEATS)-HiBiT fusion protein.[33] These efforts resulted in the identification of compound **1**, an amido-imidazopyridine inhibitor of the ENL YEATS domain (Figure 1b−d, Table 1).

Table 1. Potency of Imidazopyridine Compounds in Biochemical and Cell-Based Assays

compound	ENL-H3K27cr HTRF IC_{50} (μM)	ENL(YEATS)-HiBiT CETSA EC_{50} (μM)
1	7.0	9.0
2	>50	>20
3	0.087	3.0
5	3.6	
6	13.0	
7	0.232	1.5
9	0.007	0.425
10 (SR-0813)	0.025	0.205

To better gauge the suitability of this scaffold for further optimization, we sought to identify preliminary evidence of a structure−activity relationship (SAR). Methylation of the amide (**2**) resulted in complete ablation of activity against ENL YEATS, whereas exchanging the isopropyl for a cyclobutyl group (**3**) greatly improved potency by both HTRF and CETSA (Figure 1b−d, Table 1). Compounds **1** and **3** also inhibit the YEATS domain of AF9, the closest homologue of ENL,[13] but do not affect the first bromodomain of BRD4 (Figure S1a,b). Finally, limited exploration of the phenyl ring did not yield any notable improvements but did establish the meta and para positions as permissible sites for substitution. We speculated that these sites might tolerate linker attachments for the design of PROTACs to degrade ENL. PROTACs are heterobifunctional small molecules that recruit a target protein to an E3 ubiquitin ligase complex to elicit ligand-dependent protein degradation.[35] Ultimately, we considered that the discovery of a selective degrader from this scaffold would substantiate ENL as an authentic target of the imidazopyridine series.

Using a polyethylene glycol linker, we attached **3** to thalidomide, which binds to the E3 substrate adapter, cereblon (CRBN), to yield SR-1114 (**4**). In MV4;11 cells, SR-1114 elicits rapid, CRBN-dependent degradation of ENL with a half-maximal degradation concentration (DC_{50}) of 150 nM (Figures 1e,f and S1c). At a concentration of 10 μM, maximal degradation occurs within 4 h but is only sustained by a single dose for 24 h (Figure S1d,e). After withdrawal of SR-1114 from cells, ENL is rapidly resynthesized within 24 h (Figure S1f). ENL is also degraded by SR-1114 in MOLM-13 (DC_{50} = 311 nM) and OCI/AML-2 (DC_{50} = 1.65 μM) cell lines (Figure S1g,h), altogether confirming that the imidazopyridine series can support the development of effective ENL PROTACs.

We evaluated the selectivity of SR-1114-induced ENL degradation by mass spectrometry (MS)-based expression proteomics using isobaric tandem mass tag (TMT) labeling for quantification. After 4 and 16 h exposures of MV4;11 cells to SR-1114 (10 μM), ENL showed the strongest change in abundance across the proteome (Figure 1g, Table S1). Since AF9 is not expressed in MV4;11 cells and therefore not detected by proteomics, this experiment did not reveal if SR-1114 can also degrade AF9. Our attempts to unambiguously detect AF9 by immunoblot in other cell lines were unsuccessful, so we expressed AF9 with a carboxy-terminal V5 epitope tag in MOLM-13 cells. This enabled detection of exogenously expressed AF9 and confirmed that it is degraded by SR-1114 (Figure S1i). After 16 h, SR-1114 treatment resulted in the preferential suppression of multiple ENL target genes, including HOXA10, MYC, MYB, FLT3, ZEB2, and SATB1 (Figure 1h, Table S1), closely replicating the transcriptional consequences of dTAG-mediated ENL degradation.[10] Furthermore, the 16 h SR-1114 treatment also increased the abundance of the myeloid differentiation marker, CD11b, in agreement with the proposed role for ENL in preventing the terminal differentiation of AML cells.[11] These data elevated our confidence in ENL as a leukemia target and simultaneously provided an orthogonal validation of ENL as a target of the amido-imidazopyridine series.

Unfortunately, proteomics studies also revealed weak off-target degradation of the IKAROS family transcription factor, IKZF1 (Figure 1g,h). Thalidomide is known to induce the degradation of IKZF1 by recruiting it to CRBN[36,37] and, in some instances, has been observed to retain this activity even when incorporated into a PROTAC.[38,39] Since IKZF1 is a transcription factor of known importance in hematological cell types, its degradation might complicate the study of ENL-dependent transcriptional control in acute leukemia. Therefore, we decided not to proceed with further cell-based studies of SR-1114 and instead pursued enhancements in ligand affinity that would enable studies of ENL YEATS domain function in living systems.

Additional improvements to the imidazopyridine series were discovered using a high-throughput hit-to-lead process that leverages sulfur(VI) fluoride exchange (SuFEx) "click" transformations for parallelized chemical diversification (Figure 2a).[34] Capitalizing on the high-yielding reaction of iminosulfur oxydifluoride SuFEx hubs with primary and secondary amines,[38] a diverse library of sulfamide- or sulfuramidimido-

https://doi.org/10.1021/acscentsci.0c01550
ACS Cent. Sci. 2021, 7, 815−830

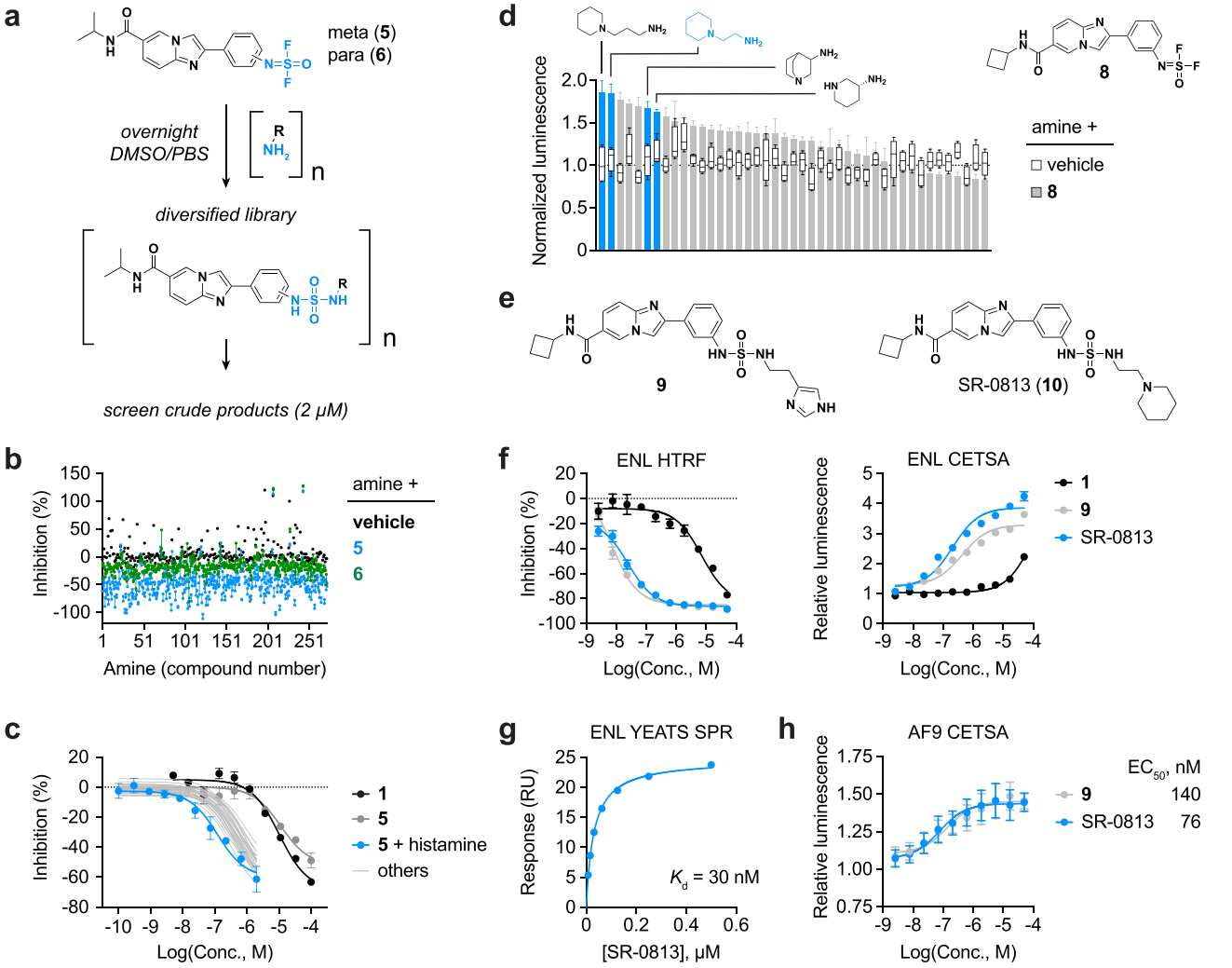

Figure 2. Hit optimization by SuFEx-based high-throughput medicinal chemistry. (a) Scheme for the highly parallel medicinal chemistry approach. Iminosulfur oxydifluoride SuFEx hubs react with primary (shown) and secondary (not shown) amines to assemble a diverse collection of near derivatives that can be tested as crude reaction products. (b) ENL YEATS HTRF assay to measure the activity of 288 amines reacted with vehicle (n = 1), **5** (n = 2), or **6** (n = 2). Individual replicates are connected by a vertical line. (c) Measurement of dose−response activity for 28 hits in the screen, testing crude reaction products by ENL YEATS HTRF. Mean ± s.e.m., n = 2. (d) Activity of crude SuFEx reaction products measured in living cells by the ENL(YEATS)-HiBiT target engagement assay. DMSO-normalized luminescence of focused amine library reacted with **8** (mean ± s.e.m., n = 4) or vehicle (box and whiskers, min to max, n = 4). (e) Chemical structures of **9** and SR-0813 (**10**). (f) Activity of **9** and SR-0813 by the HTRF (left) and ENL(YEATS)-HiBiT target engagement assay (right). Mean ± s.e.m., n = 4. (g) Binding curve for SR-0813 and ENL YEATS determined by SPR. RU, response units. (h) Engagement of AF9(YEATS)-HiBiT measured by ligand-induced luminescence. Signal normalized to DMSO ± s.e.m., n = 4.

yl-fluoride-linked analogs can be rapidly assembled in miniaturized formats.[34] Importantly, the biocompatible nature of these reactions permits testing of the crude products directly in biochemical assays without the need of further purification.[34] Without a crystal structure to guide iterative medicinal chemistry efforts, we attempted to expedite empirical discovery of optimized ENL ligands using this approach.

First, since fluoride is produced as a byproduct of the SuFEx click reactions, we tested whether it would impact the performance of the HTRF assay for ENL YEATS. Planning to screen crude reaction products at concentrations no higher than 2−5 μM, we tested the effect of adding 10 μM KF to the assay. Neither the signal window of the assay nor the Z′-factor, a statistical measure of the ability to call hits from high-throughput screening data,[39] was affected by the presence of KF (Figure S2a). To proceed with SuFEx-based diversification, we appended iminosulfur oxydifluoride groups to the meta (**5**) and para (**6**) positions on the phenyl ring of **1**. Both compounds retained activity against the ENL YEATS domain by HTRF, despite suffering minor losses compared to **1** (Figure S2b, Table 1). We then reacted each compound in parallel with a library of 288 primary and secondary amines and screened the crude products at a putative concentration of 2 μM (Figure 2a,b). In general, meta substitutions seemed to be preferred over para, and while the parent molecules are inactive at 2 μM (Figure S2b), several crude reaction products fully inhibited ENL YEATS at this presumed dose (Figure 2b, Table S2).

Selecting 28 crude products for dose−response examination, we observed striking improvements in potency compared to the parent molecule (Figure 2c, Table S3). The most potent hit, formed by the reaction of **5** with histamine, inhibited ENL

https://doi.org/10.1021/acscentsci.0c01550
ACS Cent. Sci. 2021, 7, 815−830

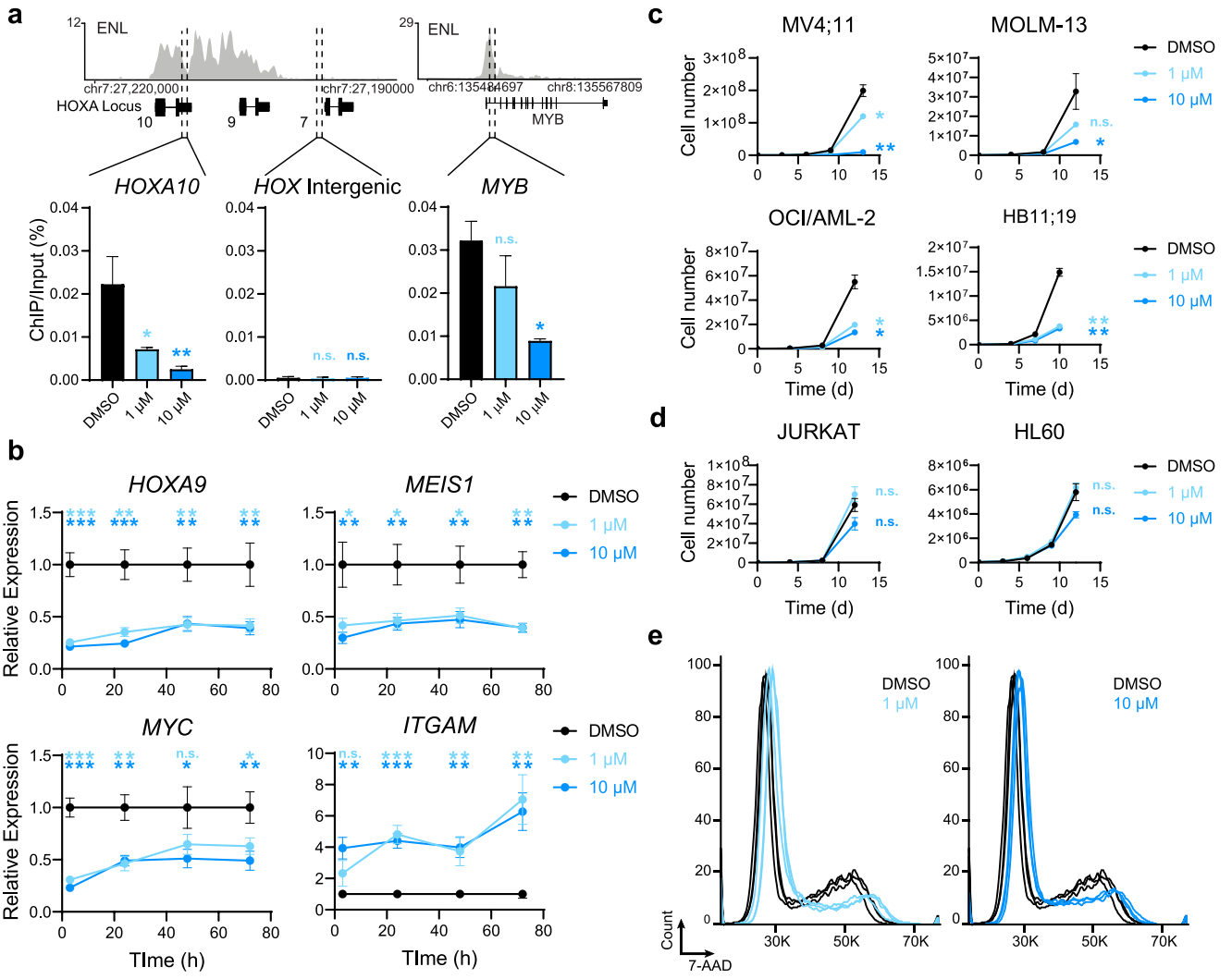

Figure 3. On-target effects of SR-0813 in leukemia. (a) ENL displacement from chromatin by SR-0813. Top: gene track views of the ENL ChIP-seq signal from DMSO treated MV4;11 cells. Bottom: ChIP-qPCR signal in response to the SR-0813 treatment. Mean ± s.d. *P* values by Student's *t*-test compared to the DMSO sample. (b) Change in transcript abundance in MV4;11 cells treated with SR-0813 (normalized to DMSO). qRT-PCR, $n = 3$, *P* values by Student's *t*-test to DMSO sample. (c) Proliferation of MLL-fusion leukemia cell lines in response to SR-0813. Mean ± s.e.m. $n = 3$. Student's *t*-test to DMSO sample. (d) Proliferation of ENL-insensitive acute leukemia cell lines in response to SR-0813. *P* values by Student's *t*-test. (e) Cell cycle analysis of MV4;11 cells treated with DMSO or SR-0813 for 72 h. $n = 3$. $^{*}P < 0.05$, $^{**}P < 0.01$, $^{***}P < 0.001$, and $^{****}P < 0.0001$. Not significant (n.s.) $P > 0.05$.

YEATS with an IC_{50} of 120 nM by HTRF (Figure 2c). To confirm this result, the compound was resynthesized, purified, and then tested for activity against ENL YEATS (**7**, Figure S2c). By HTRF, the potency of the purified product matched closely with the results obtained for the crude (IC_{50} = 230 nM; Figure S2d; Table 1). Compared to the initial screening hit (IC_{50} = 7 μM), this represents a 30-fold improvement in potency achieved in a single experiment. Nevertheless, the dramatic improvement in potency in the HTRF assay did not translate to similar gains in cell-based target engagement (EC_{50}, **1** = 9 μM; EC_{50}, **7** = 1.5 μM; Figure S2e; Table 1).

Hoping to improve the performance of **7** in cells, we speculated that SuFEx-based screening might be sufficiently biocompatible to permit the testing of crude products directly in living cells. If so, we could couple parallelized SuFEx diversification with cell-based measures of target engagement. By this time, we had discovered the improvement in potency afforded by the cyclobutylamine modification in compound **3**, so we installed the iminosulfur oxydifluoride group onto the meta position of **3** instead of **1**, yielding compound **8** (Figure 2d). This SuFEx-compatible analog was then reacted in parallel with a small collection of amines sterically related to histamine and screened for target engagement in cells at 2 μM. A noticeable preference for piperidine analogs was revealed by this experiment, including one with the same CH_2CH_2 linker as the histamine in **7** (Figure 2d, Table S4). To compare the imidazole and piperidine analogs directly, we synthesized and purified compounds **9** and **10** (SR-0813) (Figure 2e). While **9** features superior potency in the HTRF assay (IC_{50}, **9** = 7 nM; IC_{50}, SR-0813 = 25 nM), SR-0813 engages the ENL YEATS domain more potently in cells and elicits a greater E_{max} (Figure 2f, Table 1). Consistent with its 25 nM potency in the HTRF assay, we determined a 30 nM affinity between SR-0813 and the ENL YEATS domain by surface plasmon resonance (SPR)

https://doi.org/10.1021/acscentsci.0c01550
ACS Cent. Sci. 2021, 7, 815−830

(Figures 2g and S2f). Moreover, the inhibition of ENL YEATS by SR-0813 was not affected by the addition of KF, supporting the previous observation that fluoride byproduct does not affect the HTRF assay (Figure S3a). These data demonstrate that SuFEx-based high-throughput medicinal chemistry, previously applied to an inhibitor of the bacterial cysteine protease, SpeB,[34] is extensible to other targets. Equally important, we find that the approach is compatible with cell-based drug discovery.

Encouraged by the improved activity of SR-0813, we tested it for activity against all other YEATS domain proteins in humans: AF9, YEATS2, and YEATS4. As expected, both HTRF (IC_{50} = 311 nM) and CETSA (EC_{50} = 76 nM) revealed SR-0813 as a potent inhibitor of the AF9 YEATS domain (Figures 2h and S3b). While the IC_{50} values determined by HTRF suggest a preference for ENL (25 nM) over AF9 (311 nM), we noted previously that the AF9 assay reports artificially high IC_{50} values.[33] Since both targets are potently engaged in cells (EC_{50}, ENL = 205 nM; EC_{50}, AF9 = 76 nM), SR-0813 is not selective for ENL over AF9. In contrast, SR-0813 is highly selective against the YEATS domains of YEATS2 and YEATS4. To assess the selectivity against YEATS2, we used modified histone peptide arrays to detect YEATS domain recognition of immobilized acetyllysine substrates. Whereas ENL recognition of acetyllysine is completely inhibited by 1 μM SR-0813, concentrations as high as 10 and 50 μM had minimal effects on YEATS2 (Figure S3c−f, Table S5). Likewise, virtually no binding to the YEATS4 YEATS domain was observed by SPR (Figure S3g,h).

We also profiled SR-0813 for off-target effects on bromodomain proteins, the largest class of acetyllysine readers. SR-0813 was inactive in the BRD4 BD1 HTRF assay, and not a single bromodomain off target was identified using the BROMO*scan* profiling service from DiscoverX (*bromo*MAX; 32 bromodomains; Figure S4a,b; Table S6). Given the similarity of its imidazopyridine core to many bicyclic kinase inhibitors, we also tested SR-0813 for kinase off-targets using the KINOME*scan* profiling service (*scan*MAX, 468 kinases, Figure S4c, Table S7). Of the 468 kinases tested, 4 were identified as potential off targets, but subsequent affinity determination revealed 3 of these as false-positive hits (Figure S4c,d). The remaining kinase, YSK4 (also known as MAP3K19), was bound by SR-0813 with over 100-fold lower affinity (K_d = 3.5 μM) than ENL YEATS and would not be expected to complicate studies of ENL function in cellular model systems. Altogether, these studies suggest SR-0813 is a highly selective and potent dual inhibitor of the ENL/AF9 YEATS domains.

Enabled by the discovery of SR-0813, we sought to characterize the effects of ENL/AF9 YEATS domain inhibition in cells. Previously, alanine substitutions in the ENL YEATS domain helped to establish acyl-lysine recognition as an important contributor to ENL chromatin localization.[10,11] To test this model via direct pharmacological occupation of the ENL YEATS domain, we preformed chromatin immunoprecipitation (ChIP) of ENL following treatment of MV4;11 cells with SR-0813 for 4 h. Quantification of ChIP enrichment by qPCR demonstrated clear dose-dependent eviction of ENL from known ENL binding sites, including the *HOXA10* gene body and *MYB* promoter (Figure 3a). Not knowing whether this effect is sufficient to suppress the expression of ENL target genes, so we measured the impact of SR-0813 on known ENL targets, *HOXA9*, *MEIS1*, and *MYC*.[10] Each gene was downregulated in response to SR-0813, beginning as early as 3 h after drug exposure and sustained for at least 3 days (Figure 3b). We also observed an increased abundance of the *ITGAM* transcript, which encodes for CD11b (Figure 3b), consistent with previous RNA-seq studies that measured the effects of dTAG-mediated ENL degradation in MV4;11 cells.[10] As noted above, CD11b protein abundance is also elevated in MV4;11 upon SR-1114 treatment (Figure 1h) and in MOLM-13 cells upon genetic depletion of ENL.[11] Taken together, these data support the hypothesis that ENL/AF9 YEATS inhibition is sufficient to disrupt ENL function in living AML cells. Interestingly, 1 and 10 μM doses appear equally capable of suppressing ENL target genes (Figure 3b), despite the more effective displacement of ENL from chromatin at 10 μM (Figure 3a).

After confirming the most proximal biomarkers of ENL YEATS engagement by SR-0813, we next characterized its effect on acute leukemia proliferation, comparing it to the known pattern of sensitivity to ENL depletion by CRISPR/Cas9. We began by testing the viability of MV4;11 cells following 72 h SR-0813 treatments but observed minimal effects (Figure S5a). We considered that like DOT1L, a related epigenetic target in MLL-fusion leukemia, ENL disruption may require longer than 72 h to derive an antileukemic effect.[40] Therefore, we tested the effect of extended SR-0813 treatments on AML cells over a period of ∼2 weeks, beginning with 3 MLL-fusion leukemia that were previously shown to be sensitive to the genetic loss of ENL, MV4;11 (MLL-AF4 AML), MOLM-13 (MLL-AF9 AML), and OCI/AML-2 (MLL-AF6 AML).[10,11] SR-0813 inhibited the growth of each of these three cell lines as well as HB11;19 cells, which have not been tested for their reliance on wild-type ENL but harbor an MLL-ENL fusion (Figure 3c). In contrast, the growth patterns of JURKAT (T-cell ALL) and HL-60 (MLL wild-type AML) cells, both of which are insensitive to ENL loss,[10] are unaffected by SR-0813 (Figure 3d). Additionally, neither the T-cell ALL cell line, MOLT-4, nor the renal cell carcinoma cell line, 786-O, were affected by SR-0813 (Figure S5b,c). Although these cell lines have not been tested for their reliance on ENL, these data support the conclusion that SR-0813 is not promiscuously toxic, even at concentrations as high as 10 μM. Moreover, we determined that the inhibition of MV4;11 growth by SR-0813 is accompanied by a decrease in the number of cells at the G2 stage of the cell cycle (Figure 3e), in line with previous data demonstrating G1 arrest upon loss of ENL.[10,11] Unfortunately, SR-0813 is rapidly metabolized by mouse liver microsomes ($t_{1/2}$ = 9.3 min, R^2 = 0.9996, Figure S5d), prohibiting the extension of these findings in vivo. Taken together, these data are fully consistent with the pattern of sensitivity to genetic disruption of ENL, supporting the hypothesis that on-target effects are responsible for SR-0813-mediated inhibition of ENL-dependent leukemia growth.

Among AML cell lines that are sensitive to SR-0813, we noticed differences in the response to 1 μM SR-0813 (Figure 3c). Initially, MV4;11 cells appeared to show a dose-dependent response to SR-0813 and so did MOLM-13 cells, albeit to a lesser extent. In contrast, OCI/AML-2 and HB11;19 cells responded to 1 μM equally as well as 10 μM. Given this discrepancy, we repeated the growth assays for MV4;11 cells an additional 4 times. In each of these repeats, 1 μM SR-0813 treatments inhibited the growth of MV4;11 cells to the same extent as 10 μM treatments (Figure S5e). We also repeated the experiments an additional 5 times for HL-60 cells and once

https://doi.org/10.1021/acscentsci.0c01550
ACS Cent. Sci. 2021, 7, 815−830

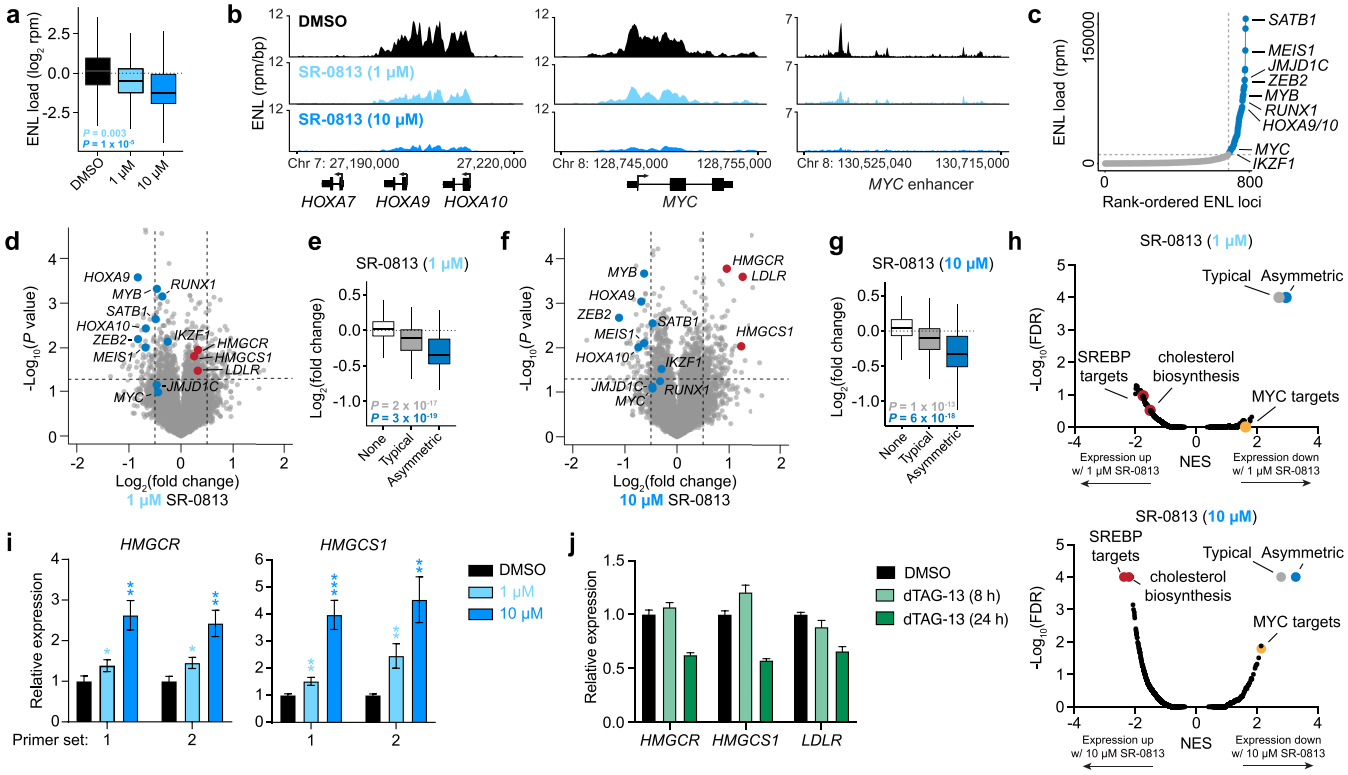

Figure 4. Selective suppression of ENL target genes by SR-0813. (a) Boxplots of the ChIP-seq signal at ENL-bound loci (n = 2152) from MV4;11 cells treated with DMSO or SR-0813. (b) Gene tracks of the ENL ChIP-seq signal at examples of the ENL-bound loci. (c) Rank-ordered plot of the ENL ChIP-seq signal at ENL peaks showing asymmetry in ENL binding to target genes. (d) Volcano plot of DMSO-normalized gene expression changes in MV4;11 cells treated with 1 μM SR-0813 for 4 h. P value calculated with two-tailed Student's t-test (n = 3). (e) Boxplots of gene expression changes with 1 μM SR-0813 at genes not bound by ENL (white, n = 12 163), typical ENL target genes (gray, n = 197), and asymmetrically loaded ENL target genes (blue, n = 74). P values calculated with Welch's two sample t-test. (f) Same as in (d) but for 10 μM SR-0813. (g) Same as in (e) but for 10 μM SR-0813. (h) Gene set enrichment analysis (GSEA) of gene-expression changes induced by a 4 h SR-0813 treatment (top: 1 μM; bottom: 10 μM). (i) Change in transcript abundance in MV4;11 cells treated SR-0813 (normalized to DMSO). qRT-PCR, n = 3, P values determined by the Student's t-test to DMSO sample. *P < 0.05, **P < 0.01, ***P < 0.001, and ****P < 0.0001. Not significant (n.s.) P > 0.05. (j) Change in transcript abundance determined by the analysis of RNA-seq performed on MV4;11 cells treated with dTAG-13 (GEO accession GSE82117).

more for JURKAT cells, confirming the muted antiproliferative activity of SR-0813 in ENL-insensitive leukemia cells (Figure S5f,g). Overall, these data indicate that 1 μM SR-0813 is sufficient to suppress ENL target gene expression and ENL-dependent leukemia growth, even though it does not fully displace ENL from chromatin.

To more fully assess the impact of SR-0813 on gene regulation in MV4;11 cells, we integrated genomic measures of ENL chromatin localization with dynamic gene expression profiling. ChIP followed by next generation DNA sequencing (ChIP-seq) revealed bulk displacement of ENL from chromatin upon treatment with SR-0813 (Figure 4a). The magnitude of ENL displacement genome-wide followed a similar dose−response pattern as was observed by ChIP-qPCR and in CETSA-based target engagement assays (Figures 2f, 3a, and 4a). This is readily apparent both genome-wide and at specific sites that are relevant to AML pathogenesis, like the *HOXA* cluster, *MYC* promoter, and *MYC* enhancer (Figures 4a,b and S6a). In previous work, we noted an asymmetric distribution of ENL on the genome whereby a small percentage of sites are occupied by a disproportionately large amount of ENL.[10] These genes, in addition to being enriched with disease-relevant leukemia proto-oncogenes, are preferentially sensitive to the acute loss of ENL by dTAG-mediated degradation. Here, we again detected this asymmetry in ENL localization (Figure 4c, Table S8) and used 3′ mRNA sequencing to determine whether asymmetrically loaded ENL target genes are differentially sensitive to SR-0813. After a 4 h exposure in MV4;11 cells, SR-0813 did not elicit global changes in gene expression, as expected (Figure 4d−g, Table S9). In contrast, it produced a strikingly selective suppression of ENL target genes with even more pronounced effects on those with disproportionate loads of ENL (Figure 4e,g). These genes include an impressive collection of transcription factors with well-established roles as leukemia drivers, including HOXA9/10, MEIS1, MYC, MYB, and ZEB2 (Figure 4d,f).[8,41−44] Since AF9 is not expressed in these cells, we can confidently ascribe these effects as the consequence of disrupting ENL function. Therefore, we show for the first time that inhibition of the ENL YEATS domain can selectively suppress leukemogenic transcriptional control by ENL.

On the basis of the previous observation that 1 μM SR-0813 is sufficient to inhibit individual ENL target genes but not fully displace ENL from chromatin, we compared the impact of 1 and 10 μM SR-0813 across the entire transcriptome. The effects of 1 and 10 μM were highly correlated (r = 0.58) and inhibited ENL target genes to the same extent (Figure S6b−d). This demonstrates on a global scale that incomplete removal of ENL by 1 μM SR-0813 is sufficient to suppress ENL-dependent transcription. Since 1 μM is also sufficient to inhibit

https://doi.org/10.1021/acscentsci.0c01550
ACS Cent. Sci. 2021, 7, 815−830

the growth of ENL-dependent leukemia, this potentially indicates that full target coverage would not be required to achieve a therapeutic effect with any clinical candidates developed in the future.

To contextualize the selectivity of SR-0813-induced transcriptional effects for ENL target genes and search for potential off-target effects, we applied an unbiased gene set enrichment analysis (GSEA) to the 3′ mRNA-seq data set. When typical and asymmetric ENL targets were profiled along with 5552 other gene sets in the molecular signatures database (MSigDB), ENL targets were by far the most highly enriched gene sets (Figure 4h, Table S10). ENL targets were enriched in both 1 and 10 μM data sets, but the effect was markedly more selective at 1 μM. At 10 μM, a number of other genes sets were also enriched, including one related to *FLT3* internal tandem duplications (ITD)[45] (a pathogenic alteration that is present in MV4;11 cells) and MYC targets (Figures 4h and S6e,f). Most notably, multiple gene sets related to cholesterol biosynthesis and SREBP (sterol regulatory element binding proteins) targets were also enriched by 10 μM SR-0813 but not by 1 μM (Figures 4h and S6e−h). In contrast to ENL targets, which are inhibited by SR-0813, SREBP targets were elevated, including *3-hydroxy-3-methylglutaryl-CoA synthase 1* (*HMGCS1*), *HMG Co-A reductase* (*HMGCR*), and *low density lipoprotein receptor* (*LDLR*) (Figure 4d,f). We confirmed the upregulation of *HMGCR* and *HMGCS1* by qRT-PCR, again observing that the effect is most prominent at 10 μM (Figure 4i). Since ENL target genes are fully suppressed by 1 μM SR-0813, we considered that this may reflect an off-target activity of the compound when used at high concentrations. To test this, we analyzed the effect of dTAG-based disruption of ENL on the same SREBP targets using a previously published RNA-seq data set (GEO accession GSE82117).[10] Neither *HMGCR*, *HMGCS1*, nor *LDLR* was upregulated by dTAG-based ENL degradation, confirming the off-target nature of the effect (Figure 4j). Fortunately, the impact of SR-0813 on SREBP targets is most apparent at 10 μM, whereas ENL targets and ENL-dependent leukemia growth are fully suppressed at 1 μM. Therefore, as a precaution, we recommend using SR-0813 at 1 μM to study ENL leukemia biology. Collectively, these unbiased data show that SR-0813-dependent changes in gene expression are exceptionally selective for ENL target genes, especially at a concentration of 1 μM. We interpret this as strong support for SR-0813 as an exquisitely selective chemical probe for the ENL YEATS domain. In characterizing the transcriptional suppression of ENL target genes, we confirm that the pharmacologically tractable ENL YEATS domain is a functionally relevant drug target in acute leukemia.

DISCUSSION

In this study, we report on the discovery of SR-0813, a highly potent and selective chemical probe for ENL/AF9 YEATS domains. Our ligand discovery efforts were motivated by the previous identification of ENL as a critical dependency in acute leukemia.[10,11] Using genetic tools to characterize this dependency *in vitro* and *in vivo*, we and others formulated the hypothesis that chromatin-competitive inhibition of the ENL YEATS domain would selectively inhibit the growth of ENL-dependent acute leukemia.[10,11] While multiple reports of synthetic YEATS domain ligands have since followed,[28−33] none have been used to address this hypothesis by studying ENL-dependent transcriptional control or ENL-dependent leukemia proliferation. In characterizing SR-0813, we provide the first pharmacological validation of ENL as a leukemia target, reproducing key mechanistic insights made in the index target identification studies. Moreover, we provide the first evidence that ENL YEATS inhibition is sufficient to inhibit ENL-dependent transcriptional control and ENL-dependent leukemia growth, confirming that this druggable domain is also functionally relevant to ENL-associated pathogenesis.

SR-0813 was elaborated from a high-throughput screening hit using an innovative high-throughput medicinal chemistry approach that leverages SuFEx reactivity to expedite chemical diversification. The conditions of these SuFEx transformations are highly biocompatible, enabling crude products to be tested directly in biochemical assays.[34] We expand on this approach by demonstrating that it is extensible to other protein targets as well as cell-based measures of small-molecule activity, which should prove highly enabling for a number of cell-based drug discovery applications. It should prove particularly useful for the optimization of phenotypic screening hits before target identification studies are able to make structure-based drug design possible. In our case, since the most potent compound in biochemical assays was not the most potent in cellular assays, the ability to measure and optimize cell-based activity was essential.

We were previously able to study the impact of ENL on leukemia gene control by using the dTAG system to elicit acute ENL degradation.[10] These studies established ENL as a highly selective transcriptional coactivator that disproportionately affects the expression of several leukemia proto-oncogenes. The use of the dTAG system in advance of embarking on a drug discovery campaign provided our group with a unique ability to anticipate the on-target effects of direct-acting ENL YEATS inhibitors. That is, we used the mechanistic insights from dTAG-based studies to benchmark the effects of our compounds on known aspects of ENL target biology. The success of this approach underscores the value of dTAG technology for target identification studies. Now equipped with a well-characterized chemical probe, we and others will be able to disrupt ENL function in a much broader range of systems than is possible with the dTAG system, which requires extensive biological engineering and relies on the expression of a tagged construct.

Here, we studied ENL-dependent gene control with direct-acting small molecules for the first time, integrating dynamic and unbiased measures of chromatin structure and function. In fact, this is the first study to demonstrate that small molecules can displace endogenous ENL from chromatin, as previous studies judged target engagement with exogenous over-expression of tagged constructs and luminescence-based proximity reporters that require hyperacetylation of the genome via pan-HDAC inhibition.[29] Since not all acetyllysine reader domains mediate chromatin localization of their host proteins (e.g., the bromodomains of SMARCA2/4 and CBP/p300),[22,46] this provides an important insight into function of the ENL YEATS domain.

Importantly, our study provides the first demonstration that inhibition of its YEATS domain is capable of disrupting ENL-dependent transcriptional control. Compared to over 5000 other gene sets, ENL targets are clearly the most severely affected class of genes to be perturbed by SR-0813. Moreover, the group of asymmetrically loaded ENL target genes, which were previously found to be hypersensitive to dTAG-mediated ENL degradation, was found to also be hypersensitive to SR-0813 treatment. This represents the first evidence that direct-

https://doi.org/10.1021/acscentsci.0c01550
ACS Cent. Sci. 2021, 7, 815−830

acting chemical tools can reproduce the genetic studies that established ENL as a selective transactivator of leukemia gene expression.

In replicating past genetic experiments, we simultaneously reinforce the evidence for ENL as a compelling leukemia dependency and validate SR-0813 as a useful chemical probe to study ENL/AF9 YEATS domain biology. Given that SR-0813 sensitivity stratifies with the known pattern of sensitivity to genetic disruption of ENL, we strongly favor the hypothesis that SR-0813 growth effects are on-target. Nevertheless, definitive confirmation of this hypothesis will ultimately require the discovery of mutant ENL alleles, or other pathway-based alterations, that rescue SR-0813 sensitivity.[47] In the meantime, we anticipate that SR-0813 and SR-1114 will represent timely additions to the collection of tools available for studying ENL and AF9 YEATS domains, as many aspects of ENL biology remain poorly understood. For instance, ENL stands in contrast to the activity of many other coactivators that act as more global regulators of gene control. For instance, BRD4, an analogous acetyllysine reader and AML target, is universally required for active gene transcription.[42,48,49] While the selectivity of ENL-dependent gene control in AML tracks with its asymmetric localization on the genome, it is still not understood how that asymmetry is established. Our molecules will help to address these and other questions, which will broaden our understanding of the role that druggable coregulators play in driving pathogenic gene control.

METHODS

Protein Production. ENL and YEATS4 YEATS domains were recombinantly expressed and purified exactly as previously described in detail.[33] Briefly, ENL(1−148) was cloned into a modified pET21a (Novagen) expression vector with an N-terminal StrepII-SUMO or SUMO-AviTag and a C-terminal 6xHis tag and expressed in BL21(DE3) cells (New England Biolabs) by isopropyl-β-D-thiogalactopyranoside (IPTG) induction (0.4 mM) at 25 °C for 20 h. After purification by metal affinity chromatography (NiNTA agarose, Qiagen), buffer exchange to 100 mM Tris-HCl at pH 8.0, 150 mM NaCl, 1 mM EDTA, and 1 mM DTT using PD10 desalting columns (GE Life Sciences), and cleavage from SUMO by Ulp1 digestion, ENL YEATS(1−148) was recovered from the flow through of a StrepTrap column (GE Life Science). YEATS4(13−158) was cloned into pET28a with an N-terminal 6xHis and a C-terminal AviTag and expressed in BL21(DE3) cells by IPTG induction (0.25 mM) at 16 °C for 20 h. After purification by metal affinity chromatography (TALON Cobalt Resin, Takara) and buffer exchange to 50 mM sodium phosphate (pH 7.4) and 150 mM NaCl using Amnicon Ultracel 10K desalting columns (GE Life Sciences), YEATS4(13−158) was recovered by size exclusion chromatography using a HiLoad Superdex column (GE) on an AKTA pure (GE). To produce biotinylated protein, BL21(DE3) cells were cotransformed with the AviTag fusions and a biotin ligase expression vector, pBirAcm (Avidity). AF9 and YEATS2 YEATS were purchased from ActiveMotif (Cat. Nos. 81124 and 81099), and BRD4 BD1 was purchased from Cayman (Cat. No. 11720)

Cell Lines. MV4;11 (RPMI 1640 supplemented with 10% fetal bovine serum (FBS), penicillin, and streptomycin), MOLM-13 (RPMI 1640 supplemented with 10% FBS, penicillin, and streptomycin), OCI/AML-2 (RPMI 1640 supplemented with 10% FBS, penicillin, and streptomycin), JURKAT (RPMI 1640 supplemented with 10% FBS, penicillin, and streptomycin), and HL-60 (RPMI 1640 supplemented with 20% FBS, penicillin, and streptomycin) cells were provided by the laboratory of Prof. James E. Bradner. 786-O (RPMI1640 + 10% FBS, penicillin) cells were provided by the laboratory of Prof. Luke L. Lairson. HB11;19 (RPMI 1640 supplemented with 10% fetal bovine serum (FBS), penicillin, and streptomycin) cells were provided by Prof. Akihiko Yokoyama. MV4;11 CRBN−/− and MOLT4 (RPMI 1640 + 10% FBS, penicillin, and streptomycin) cells were provided by Prof. Georg E. Winter.[50] All cell lines were periodically (two to four times annually) tested for mycoplasma infections and never tested positive.

HTRF. AF9 YEATS, BRD4 BD1, and ENL YEATS HTRF assays were performed exactly as previously described.[33] All assays were conducted by combining recombinant AF9 YEATS (5 nM), BRD4 BD1 (10 nM), or ENL YEATS (5 nM) with synthetic histone peptide (100 nM $H3_{13-32}$K27cr custom synthesized by ABclonal, 13.3 nM tetra-acetylated H4 from BioVision Cat. No. 7144−01, or 13.1 nM $H3_{13-32}$K27cr, respectively), 1 nM LanthaScreen Eu-anti-His Tag antibody (ThermoFisher, PV5597), and 8.9 nM SureLight allophycocyanin-streptavidin (PerkinElmer, CR130−100). For the primary screen, the assay mixture was dispensed into black 1536-well plates (Greiner HiBase) at 6 μL/well and compounds were added by acoustic transfer (Labcyte, Echo Liquid Handler). Dose−response assays were performed with 10 or 20 μL assay volumes in black 384-well low-volume plates (Corning, Cat. No. 3821), and compounds were added by pin tool transfer (Biomek FX). Compounds were incubated with the assay mixture for at least 2 h before measuring the HTRF signal on a PHERAstar plate reader (BMG Labtech; simultaneous dual emission; excitation = 337 nm; emission 1 = 665 nm; emission 2 = 620 nm). The HTRF signal was calculated as the ratio of emission 1 to emission 2. Each plate included samples treated with vehicle (DMSO) or lacking the peptide substrate, which were used to calculate the percent inhibition for compound treated wells.

Luminescence-Based CETSA. ENL(YEATS)-HiBiT and AF9(YEATS)-HiBiT constructs were stably expressed in OCI/AML-2 cells by lentiviral transduction and used for luminescence-based target engagement assays as previously described.[33] Briefly, cells were transferred to white 384-well tissue culture plates (Greiner Bio-One Cat. No. 781080) with 20 000 cells in 20 μL per well. Compounds were added by pin tool transfer (Biomek FX) and incubated for 2 h before the addition of 20 μL of Nano-Glo HiBiT Lytic Reagent (Promega, HiBiT Lytic Detection System, Cat. No. N3040) per well. Luminescence was measured after 30 min after the addition of the detection reagent using an EnVision multilabel plate reader (PerkinElmer, Model No. 2104).

SPR. Surface plasmon resonance experiments were performed on a Biacore S200 (Cytiva). A series S streptavidin sensor chip was used for ligand immobilization (Cytiva). Biotinylated ENL and biotinylated YEATS4 were prepared in HBS-EP+ buffer (10 mM HEPES, 150 mM NaCl, 3 mM EDTA, 0.05% P20, pH 7.4). Ligand immobilization was carried out in flow cells 2 and 4 with a series of ligand injections at a flow rate of 5 μL/min until the desired density was achieved (1616 RU for ENL and 2416 RU for YEATS4). Flow cells 1 and 3 were left blank as a reference. HBS-EP+ buffer with 2% DMSO was used as running buffer and for the preparation of all analyte samples with biotinylated ENL and

https://doi.org/10.1021/acscentsci.0c01550
ACS Cent. Sci. 2021, 7, 815−830

HBS-EP+ with 5% DMSO, for YEATS4. Analytes were serially diluted in polystyrene 96-well plates immediately prior to injection. Before analyte injection, 3 startup cycles were run with injections of running buffer over all flow cells. Binding data was collected by injecting the analyte at a flow rate of 30 μL/min over two flow cells (reference and immobilized ligand) at a temperature of 25 °C. The association to biotin−ENL or biotin−YEATS4 was measured over 60 s and the dissociation, over 180 s. The flow cell surfaces were regenerated with 30 s injections of running buffer over each flow cell. Duplicate injections were carried out for each sample, including the blank. Affinity curves, association and dissociation constants, and sensograms were determined using Biacore S200 evaluation software.

TMT-Based Whole Proteome Analysis. MV4;11 cells were treated with 10 μM SR-1114 for 4 or 16 h and then flash frozen. Lysis buffer is made by dissolving 1 tablet of Roche complete in 10 mL of PBS. Cells were resuspended in 150 μL of lysis buffer and sonicated (3, 10 pulses). 100 μg of protein in 100 μL of lysis buffer was used and incubated with 8 M urea (for denaturation) and 10 mM DTT (for reduction) at 65 °C for 15 min. Twenty mM iodoacetamide was then added for alkylation (37 °C, 30 min). Proteins were precipitated using the MeOH/$CHCl_3$ method (600 μL of MeOH, 200 μL of $CHCl_3$, and 500 μL of water). EPPS buffer (160 μL, 200 mM) was used to dissolve the protein pellets. Two μg of LysC was used for the first round of digestion (37 °C, 2 h), followed by the second round of trypsin digestion (5 μg, 37 °C, 16 h). 12.5 μg of peptides in 35 μL of EPPS buffer was used for TMT labeling. Three μL of TMT tags was used for each sample. The labeling was proceeded for 30 min, followed by the addition of 3 μL of TMT tags and incubation for another 30 min. The reaction was stopped by adding 6 μL of 5% hydroxylamine and 2.5 μL of formic acid.

Two μL of peptide from each group was combined for a ratio check by mass spectrometry. Peptides were then combined using the adjusted volumes based on the normalized ratios and desalted by Sep-Pak C18 cartridges. The combined peptide was fractionated into a 96-well plate. Every 12th fraction was combined. The resulting 12 fractions were dried using SpeedVac vacuum and dissolved in 15 μL of buffer A. Peptides were analyzed by liquid chromatography tandem mass spectrometry (Orbitrap Fusion mass spectrometer) coupled to an UltiMate 3000 Series LC system. The peptides were separated in a capillary column (75 μm diameter packed with Acquity BEH C18, 1.7 μm, 25 cm) at a flow rate of 0.25 μL/min following the previously reported method.[51]

Immunoblotting. Whole cell lysates were prepared by solubilization of cell pellets in CelLytic M (Sigma cat# C2978) 1× HALT protease inhibitor cocktail (Thermo) and 0.1% benzonase (EMD Millipore) by vertexing for 20 s followed by a 15 min incubation on ice. Cleared lysates were prepared by centrifugation at 18 000*g* for 11 min at 4 °C. All samples were run with the same amount of total protein as determined by a BCA protein assay Kit (Pierce). ENL (Cell Signaling Technology, #14893S), AF9-V5 (Life Technologies, Cat. No. R96025), and GAPDH (Santa Cruz Biotechnology, sc-25778) antibodies were used at a 1:1000 ratio in 5% nonfat milk in 1× TBST and detected with fluorescently labeled infrared secondary antibodies (IRDye) on the Odyssey CLx Imager (LI-COR). Quantitation was performed in ImageStudio Lite (LI-COR), and the nonlinear fit for DC_{50} determination was verified by GraphPad Prism version 8.4.3 for Windows (GraphPad Software).

DiscoverX Profiling Services. Bromodomain and kinase domain off-target effects of SR-0813 (10 μM) were profiled by the commercially available BROMO*scan* (using the bromoMAX panel of 32 targets) and KINOME*scan* (using the scanMAX panel of 468 targets) profiling services from DiscoverX.

Microsome Stability Assay. SR-0813 (1 μM) was incubated with 0.5 mg/mL human or mouse liver microsomes (Corning) at 37 °C and quantitated by LC-MS/MS (API 6500) using imipramine as an internal standard.

Modified Histone Peptide Arrays. MODified Histone Peptide Arrays (Active Motif) were blocked in 1× PBS + 0.1% Tween 20 + 1% nonfat milk (peptide array blocking buffer) for 1 h at RT with shaking. Arrays were incubated overnight with either 500 nM purified ENL YEATS domain or 1 μM YEATS2 YEATS domain (Active Motif) and treated 1:1000 with the appropriate compound stock of DMSO or DMSO in blocking buffer 4 °C with shaking. Arrays were washed 3 × 5 min in 1× PBS at 4 °C with shaking. Arrays were incubated for 2 h with 1:2000 anti-6xHis (CST) for ENL or 1:2000 anti-FLAG (M2 antibody, Sigma Cat. No. 1804) in peptide array blocking buffer at 4 °C with shaking. Arrays were washed 3× for 5 min in 1× PBS at 4 °C with shaking. Arrays were incubated at a ratio of 1:20 000 with fluorescently labeled infrared secondary antibodies (IRDye) in peptide array blocking buffer for 30 min at 4 °C and with shaking. Arrays were washed 3× for 5 min in 1× PBS 4 °C, shaken, and imaged the Odyssey CLx Imager (LI-COR). Quantitation was performed by Array Analyzer Software (Active Motif https://www.activemotif.com/catalog/668/modified-histone-peptide-array).

Cell Proliferation, Viability, and Cell Cycle Assays. Cell proliferation assays were carried out in 96-well tissue culture plates at 20 000 cells/well for all lines except for HL60s (which were started at 40 000 cells/well) in 200 μL with compounds added as 1:1000 dilutions of DMSO stocks in triplicate. Culture density was determined every 3−4 days using the Countess automated cell counter (Invitrogen), after which 20 000 live cells were reseeded in fresh media and compound. The cumulative cell count was achieved by back calculation. For the 72 h viability assay, cells were plated at 1000 cells per well in 50 μL of culture media into 384-well tissue culture plates. 100 nL of compounds in DMSO was added by pin tool transfer (Biomek FX). Plates were incubated for 72 h, and ATP-dependent luminescence was determined by the ATPlite 1 Step Luminescence Assay (PerkinElmer). Data were acquired on an EnVision multilabel plate reader (PerkinElmer, Model No. 2104). For cell cycle analysis, 500k cells were cultured at 1 mL/well in a 24-well plate treated in a ratio of 1:1000 with compound stocks in DMSO or 1:1000 with DMSO in triplicate. 7-AAD staining was performed using the FITC BrdU Flow Kit from BD Biosciences. 7-AAD signal was analyzed by flow cytometry with a NovoCyte 3000 from Agilent. Flow cytometry results were analyzed by FlowJo software (version 10.7 Becton, Dickinson and Company).

qRT-PCR. RNA extracts were prepared with the RNeasy Mini plus Kit (Qiagen). cDNA was synthesized with the SuperScript VILO cDNA Synthesis Kit (Life Technologies cat# 11755050) at 100 ng/μL RNA. cDNA was analyzed in triplicate with a 7900HT Fast Real-Time PCR System (Applied Biosystems) in SYBR Select Master Mix (Life Technologies cat# 4472908) with the primer pairs detailed

https://doi.org/10.1021/acscentsci.0c01550
ACS Cent. Sci. 2021, 7, 815−830

below. Cycle numbers (Ct) were determined by the default setting on Design and Analysis (Applied Biosystems) and converted to expression fold change by normalization to B2M transcript levels.

Primer Pairs for qRT-PCR. The primer pairs are as follows. HOXA9: forward 5′-GTATAGGGGCACCGCTTTTT-3′, reverse 5′-AATGCTGAGAATGAGAGCGG-3′. MEIS1: forward 5′-CACGCTTTTTGTGACGCTT-3′ reverse 5′-GGACAACAGCAGTGAGCAAG'3′. MYC: forward 5′-CACCGAGTCGTAGTCGAGGT-3′ reverse 5′-TTTCGGGTAGTGGAAAACCA-3′. ITGAM: forward 5′-CAAAATACTGGAGCCTGGGA-3′ reverse 5′-CCTGTTTCACGGAACCTCAG-3′. B2M: forward 5′-AATGTCGGATGGATGAAACC-3′ reverse 5′-TAGCTGTGCTCGCGCTACT-3′. HMCGR1: forward-1 5′-TGATTGACCTTTCCAGAGCAAG-3′ reverse-1 5′-CTAAAATTGCCATTCCACGAGC-3′ forward-2 5′-CGTGGAATGGCAATTTTAGGTCC-3′ reverse 5′-ATTTCAAGCTGACGTACCCCT-3′. HMGCS1: forward-1 5′-CTCTTGGGATGGACGGTATGC-3′ reverse-1 5′-GCTCCAACTCCACCTGTAGG-3′ forward 5′-CATTAGACCGCTGCTATTCTGTC −3′ reverse-2 5′-TTCAGCAACATCCGAGCTAGA-3′.

ChIP. ChIP-seq was performed as previously described.[10] For ENL ChIPs, 100 million cells were treated per condition in 100 mL. Cells were cross-linked for 10 min by rocking at RT with the addition of a 1/10th volume of 10× cross-linking solution (11% formaldehyde, 50 mM HEPES, pH 7.3, 100 mM NaCl, 1 mM EDTA, pH 8.0, 0.5 mM EGTA, pH 8.0). At the end of 10 min, cultures were quenched in 125 mM glycine, freshly made, and rocked for an additional 10 min. Cross-linked cells were then washed 3× in cold 1× DPBS, pH 7.4, and pellets were flash frozen in liquid nitrogen and stored at −80 °C. Pellets were resuspended in cold lysis buffer 1 (LB1; 5 mL per 50 million cells; 50 mM HEPES, pH 7.3, 140 mM NaCl, 1 mM EDTA, 10% glycerol, 0.5% NP-40, and 0.25% Triton X-100; 1× HALT protease inhibitor cocktail from Thermo) and rotated end over end for 10 min at 4 °C. The pellet was collected at 1350*g*, resuspended in cold lysis buffer 2 (LB2; 5 mL per 50 million cells; 10 mM Tris-HCl, pH 8.0, 200 mM NaCl, 1 mM EDTA, pH 8.0, and 0.5 mM EGTA, pH 8.0; 1× HALT protease inhibitor cocktail from Thermo), and rotated end over end for 10 min at 4 °C. Pellets were collected at 1350*g*, resuspended in 3 mL of sonication buffer (50 mM HEPES, pH 7.3, 140 mM NaCl, 1 mM EDTA, 1 mM EGTA, 1% Triton X-100, 0.1% Na-deoxycholate, 0.5% SDS; 1× HALT protease inhibitor cocktail from Thermo), split into 250 μL volumes in 1.5 mL Bioruptor Plus TPX microtubes (Diagenode, #C30010010), and sheared at 4 °C using a water bath sonicator (Bioruptor Pico, Diagenode; 25 min; 30 s on, 30 s off). Sheared lysates were cleared by centrifugation at 18 000*g* for 11 min at 4 °C and pooled. 50 μL of the cleared lysate was stored at −20 °C for isolation as the input. The remaining cleared lysate was diluted 1:5 in cold sonication buffer lacking SDS, such that the final SDS concentration was 0.1%. Magnetic protein G beads (Dynabeads, ThermoFisher Scientific) were washed 3 times in 1 mL of cold blocking buffer (1× DPBS + 5 mg/mL BSA), then resuspended in 1 mL of blocking buffer with 10 μg of anti-ENL (Cell Signaling Technology, #14893S), and rotated end over end at 4 °C overnight. Antibody-bead complexes were washed 3× in cold blocking buffer, added to the diluted cleared sonicated lysates, and rotated end over end overnight at 4 °C. The bead bound fraction was washed twice in cold sonication buffer (no SDS), once with 1 mL of cold sonication buffer supplemented with 500 mM NaCl, once with cold LiCl wash buffer (20 mM Tris, pH 8.0, 1 mM EDTA, 250 mM LiCl, 0.5% NP-40, 0.5% Na-deoxycholate), and once with TE supplemented with 50 mM NaCl. The remaining bound fraction was eluted by the addition of 210 μL of elution buffer (50 mM Tris-HCl, pH 8, 10 mM EDTA, and 1% SDS) and vortexed every 5 min while otherwise incubated at 65 °C for a total of 15 min. Beads were then centrifuged at 18 000*g* for 1 min, and the supernatant was removed; the sample was incubated overnight alongside the 50 μL input sample after the addition of 150 μL of elution buffer to bring it up to 200 μL for all samples. RNA was digested with 0.2 mg/mL RNase A (Roche, 10109169001) at 37 °C for 2 h, and protein was digested with 0.2 mg/mL proteinase K (Life Technologies, AM2546) at 55 °C for 30 min. DNA was isolated with phenol chloroform extraction and ethanol precipitation. Libraries for Illumina sequencing were prepared using the ThruPLEX DNA-seq Kit (Takara cat# R400675) with 0.75 ng of DNA and amplifying according to the manufacturer's instructions using the DNA Single Index Kit 12 Set A (Takara cat# R400695). Amplified libraries were isolated using AMPure beads (Agencourt AMPure XP). Library quantity and size distribution were determined by the Qubit 1X dsDNA HS Assay Kit (ThermoFisher cat# Q33231) and D1000 high sensitivity DNA tape run on a 4150 TapeStation System (Agilent); samples were multiplexed with equimolar DNA content and sequenced on an Illumina NextSeq 500 (single end 75 bp reads).

ChIP-qPCR. ChIP-seq DNAs from the above method were diluted and subjected to qPCR interrogation. DNA was analyzed in triplicate with a 7900HT Fast Real-Time PCR System (Applied Biosystems) in a SYBR Select Master Mix (Life Technologies cat# 4472908) with the primer pairs detailed below. Cycle numbers (Ct) were determined by the default setting on Design and Analysis (Applied Biosystems) and converted to expression fold change

ChIP-qPCR Primers. The primers are as follows. HOXA10: forward 5′-GCCGCTCTCGAGTAAGGTAC-3′, reverse 5′-GGCAAAGAGTGGTCGGAAGA-3′. HOXA_intergenic_1: forward 5′-CGCCTTCCAGAGATTTGGGT-3′, reverse 5′-TGTCTTTGCACCCAGGCTAG-3′. MEIS1_1: forward 5′-GGGAAACGCGAGCTTTTGTT-3′, reverse 5′-GGCTAGGAAGTCCGCAAAGT-3′. MYB_1: forward 5′-TGCAAAGTTCAAAGGCGAGC-3′, reverse 5′-CTTCTGCAGGACCTGAAGGG-3′.

Quant-seq. For quantitative RNA-seq, cells were treated in triplicate with 1:1000 DMSO, 10 μM SR-0813, or 1 μM SR-0813 (from the dilution of 1000× stocks in DMSO) for 4 h and harvested. 500k cells were resuspended in lysis buffer containing an ERCC spike (SIRV set 3, Lexogen cat# K05103-0-0100), and samples were isolated with an RNeasy Plus Kit from Qiagen. 400 ng of RNA was used to prepare the libraries for sequencing with the QuantSeq 3′ mRNA-Seq Library Prep Kit (FWD) for Illumina (Lexogen, cat# 015.2), and equimolar multiplexed libraries were sequenced on an Illumina NextSeq 500 (single end 75 bp reads).

ChIP-seq Analysis. ChIP data sets were aligned to human genome build hg19 with Bowtie2 (Version 2.2.9). All default settings were used except for −N 1 (allowing 1 mismatch in seed alignments). SAM alignment files were converted to BAM files with the Samtools (Version 1.9) view. BAM files were then sorted and indexed with Samtools. The model-based

https://doi.org/10.1021/acscentsci.0c01550
ACS Cent. Sci. 2021, 7, 815−830

analysis of the ChIP-seq (MACS) peak-finding algorithm (Version 1.4.2) was used to identify regions of the ChIP-seq signal that were significantly enriched over the background. The normalized read density for specific genomic loci of interest was determined using the Bamliquidator (http://github.com/BradnerLab/pipeline/wiki/bamliquidator) read density calculator. ROSE2 was used to identify regions of asymmetric ENL binding (https://github.com/linlabbcm/rose2). ChIP-seq data produced for this publication can be accessed online using GEO Publication Reference ID GSE162591.

Quant-seq Analysis. For Quant-seq analysis, the quality of sequencing data was assured with Fastqc. SlamDunk (with the −q option to ignore SLAM-seq scoring) was used to align reads to human genome build hg19 and calculate counts per million (CPM) at all 3′ UTRs. Average log2-transformed fold change values were calculated from the means of triplicate treatments. Transcripts with an average CPM < 3 were excluded from the analysis. Quant-seq data produced for this publication can be accessed online using GEO Publication Reference ID GSE162592.

Synthetic Procedures. *General.* All reagents and solvents were purchased from commercial suppliers and were used without further purification. ^{1}H, ^{13}C, and ^{19}F NMR spectra were collected using a Bruker 600, 500, or 400 MHz spectrometer with chemical shifts reported relative to residual deuterated solvent peaks or a tetramethylsilane internal standard. $CFCl_3$ was used as an internal standard for ^{19}F-NMR. Accurate masses were measured using an ESI-TOF (HRMS, Waters Xevo G2-XS TOF) or MSQ Plus mass spectrometer (LRMS, Thermo Scientific). Reactions were monitored on TLC plates (silica gel 60, F254 coating, EMD Millipore, 1057150001), and spots were either monitored under UV light (254 mm) or stained with phosphomolybdic acid. The purity of the compounds that were tested in the biological assay was >95% based on ^{1}H NMR and reverse phase HPLC-UV monitoring of the absorption at 240 nm.

Representative Procedure for the Synthesis of Imidazopyridine.

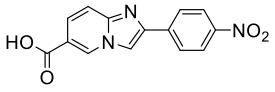

To a DMF solution of 6-aminonicotinic acid (1 g, 7.24 mmol) was added 2-bromo-4-nitroacetophenone (3.5 g, 14.5 mmol, 2 equiv), and the mixture was stirred overnight at 60 °C. The reaction mixture was cooled to RT, and ethyl acetate and water were added to this solution. The resulting precipitate was collected by filtration and then washed with water and ethyl acetate to give a fairly pure target molecule as a red powder. The compound was used in the next step without further purification (2-(4-nitrophenyl)imidazo[1,2-*a*]pyridine-6-carboxylic acid, 1.39 g, 4.9 mmol, 68%). LRMS (+) calcd for $(M + H)^+$ 284.1. Found 284.2. ^{1}H NMR (600 MHz, DMSO-d_6) δ 9.27 (t, J = 1.4 Hz, 1H), 8.76 (s, 1H), 8.36−8.32 (m, 2H), 8.23 (dd, J = 9.1, 2.4 Hz, 2H), 7.73−7.66 (m, 2H). ^{13}C NMR (151 MHz, DMSO-d_6) δ 165.8, 146.8, 145.6, 143.3, 139.7, 131.3, 126.6, 125.3, 124.3, 117.1, 116.3, 112.9.

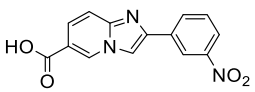

2-(3-Nitrophenyl)imidazo[1,2-*a*]pyridine-6-carboxylic acid, 1.43 g (5.1 mmol, 70%). LRMS (+) calcd for $(M + H)^+$ 284.1. Found 284.2. ^{1}H NMR (600 MHz, DMSO-d_6) δ 9.23 (t, J = 1.4 Hz, 1H), 8.76 (t, J = 2.0 Hz, 1H), 8.74 (s, 1H), 8.39 (dt, J = 7.7, 1.3 Hz, 1H), 8.20 (ddd, J = 8.2, 2.4, 1.0 Hz, 1H), 7.79−7.76 (m, 1H), 7.70−7.68 (m, 2H). ^{13}C NMR (151 MHz, DMSO-d_6) δ 165.8, 148.4, 145.4, 143.3, 135.0, 131.9, 131.2, 130.5, 125.1, 122.6, 122.4, 119.9, 116.2, 111.8.

Representative Procedure for the Amide Coupling.

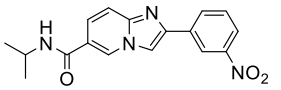

To a DMF solution of 2-(3-nitrophenyl)imidazo[1,2-*a*]-pyridine-6-carboxylic acid (1.5 g, 5.3 mmol) was added *N*,*N*-diisopropylethylamine (DIPEA, 2.8 mL, 2 g, 15.5 mmol) followed by 1-[bis(dimethylamino)methylene]-1*H*-1,2,3-triazolo[4,5-*b*]pyridinium 3-oxid hexafluorophosphate (2.4 g, 6.32 mmol, 1.2 equiv) and isopropylamine (470 mg, 8 mmol, 1.5 equiv), and the mixture was stirred overnight at RT. The solvent was removed, and ethyl acetate was added to the residue. The solid was collected by filtration and washed with ethyl acetate to give a fairly pure target molecule *N*-isopropyl-2-(3-nitrophenyl)imidazo[1,2-*a*]pyridine-6-carboxamide as a yellow powder (860 mg, 2.65 mmol, 50%). LRMS (+) calcd for $(M + H)^+$ 325.1. Found 325.2. ^{1}H NMR (600 MHz, DMSO-d_6) δ 9.11−9.04 (m, 1H), 8.78 (t, J = 2.0 Hz, 1H), 8.72 (s, 1H), 8.45−8.36 (m, 2H), 8.19 (d, J = 8.4 Hz, 1H), 7.80−7.71 (m, 2H), 7.67 (d, J = 9.6 Hz, 1H), 4.20−4.09 (m, 1H), 1.21 (d, J = 6.6 Hz, 6H). ^{13}C NMR (151 MHz, DMSO-d_6) δ 163.0, 148.4, 145.1, 143.2, 135.3, 131.9, 130.4, 128.2, 124.3, 122.5, 120.6, 119.8, 115.9, 111.5, 41.2, 22.3.

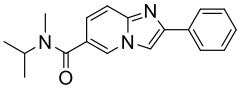

N-Isopropyl-*N*-methyl-2-phenylimidazo[1,2-*a*]pyridine-6-carboxamide (compound **2**). LRMS (+) calcd for $(M + H)^+$ 294.2. Found 294.1. ^{1}H NMR (400 MHz, DMSO-d_6) δ 8.70 (s, 1H), 8.43 (s, 1H), 7.98 (d, J = 7.5 Hz, 2H), 7.63 (d, J = 9.2 Hz, 1H), 7.46 (t, J = 7.6 Hz, 2H), 7.35 (t, J = 7.3 Hz, 1H), 7.26 (t, J = 8.9 Hz, 1H), 4.70−4.10 (broad m, 1H), 2.86 (s, 3H), 1.18 (d, J = 8.0 Hz, 6H).

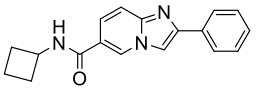

N-Cyclobutyl-2-phenylimidazo[1,2-*a*]pyridine-6-carboxamide (compound **3**). LRMS (+) calcd for $(M + H)^+$ 292.1. Found 292.1. ^{1}H NMR (400 MHz, DMSO-d_6) δ 9.06 (s, 1H), 8.73 (d, J = 7.4 Hz, 1H), 8.50 (s, 1H), 7.98 (d, J = 7.3 Hz, 2H), 7.69−7.60 (m, 2H), 7.46 (t, J = 7.6 Hz, 2H), 7.35 (t, J = 7.3 Hz, 1H), 4.47−4.41 (m, 1H), 2.27−2.21 (m, 2H), 2.11−2.05 (m, 2H), 1.73−1.65 (m, 2H).

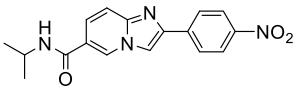

N-Isopropyl-2-(4-nitrophenyl)imidazo[1,2-*a*]pyridine-6-carboxamide. LRMS (+) calcd for $(M + H)^+$ 325.1. Found 325.2. ^{1}H NMR (600 MHz, DMSO-d_6) δ 9.09 (d, J = 1.7 Hz, 1H), 8.73 (s, 1H), 8.42−8.21 (m, 5H), 7.80−7.61 (m, 2H), 4.18−4.06 (m, 1H), 1.20 (d, J = 6.6 Hz, 6H). ^{13}C NMR (151 MHz, DMSO-d_6) δ 163.0, 146.7, 145.3, 143.2, 140.1, 128.3, 126.5, 124.6, 124.2, 120.7, 116.0, 112.6, 41.2, 22.3.

https://doi.org/10.1021/acscentsci.0c01550
ACS Cent. Sci. 2021, 7, 815−830

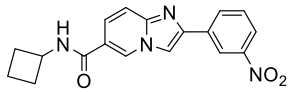

N-Cyclobutyl-2-(3-nitrophenyl)imidazo[1,2-*a*]pyridine-6-carboxamide (914 mg, 2.72 mmol, 51%). LRMS (+) calcd for $(M + H)^+$ 337.1. Found 337.2. ^{1}H NMR (600 MHz, DMSO-d_6) δ 9.08 (q, J = 1.4 Hz, 1H), 8.82−8.75 (m, 2H), 8.73 (d, J = 1.3 Hz, 1H), 8.42 (dt, J = 7.8, 1.4 Hz, 1H), 8.19 (ddt, J = 8.2, 2.5, 1.2 Hz, 1H), 7.80−7.70 (m, 2H), 7.68 (d, J = 9.4 Hz, 1H), 4.50−4.40 (m, 1H), 2.28−2.22 (m, 2H), 2.14−2.11 (m, 2H), 1.78−1.63 (m, 2H). ^{13}C NMR (151 MHz, DMSO-d_6) δ 162.9, 148.4, 145.1, 143.2, 135.3, 131.8, 130.4, 128.3, 124.3, 122.5, 120.3, 119.8, 115.9, 111.5, 44.6, 30.1, 14.8.

Representative Procedure for Reduction of Nitrophenyl into Aniline.

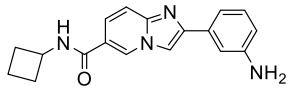

To a DMF solution of *N*-cyclobutyl-2-(3-nitrophenyl)imidazo-[1,2-*a*]pyridine-6-carboxamide (300 mg, 0.89 mmol) was added 5% Pd/C (100 mg), and the mixture was purged with H_2 gas and stirred at RT overnight. The solvent was removed, and a solution of water/acetonitrile (MeCN)/trifluoroacetic acid(TFA) (90:10:0.1) was added to the residue; it was then filtered through 0.22 μm PTFE syringe filter. The filtrate was purified by HPLC to give the target molecule 2-(3-amino-phenyl)-*N*-cyclobutylimidazo[1,2-*a*]pyridine-6-carboxamide as a white solid (135 mg, 0.44 mmol, 50%). LRMS (+) calcd for $(M + H)^+$ 307.2. Found 307.3. ^{1}H NMR (600 MHz, DMSO-d_6) δ 9.21 (s, 1H), 8.91 (d, J = 7.4 Hz, 1H), 8.59 (s, 1H), 7.97 (d, J = 9.5 Hz, 1H), 7.78 (d, J = 9.4 Hz, 1H), 7.46 (d, J = 12.0 Hz, 2H), 7.37 (t, J = 7.8 Hz, 1H), 6.96 (d, J = 7.9 Hz, 1H), 4.45 (h, J = 8.1 Hz, 1H), 2.34−2.20 (m, 2H), 2.20−1.99 (m, 2H), 1.71 (ddd, J = 15.6, 10.3, 7.4 Hz, 2H). ^{13}C NMR (151 MHz, DMSO-d_6) δ 162.3, 142.9, 140.9, 131.0, 130.2, 129.1, 127.6, 122.2, 119.1, 117.0, 115.4, 115.1, 113.7, 111.1, 44.8, 30.0, 14.8.

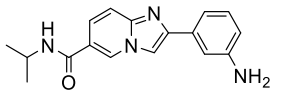

2-(3-Aminophenyl)-*N*-isopropylimidazo[1,2-*a*]pyridine-6-carboxamide. LRMS (+) calcd for $(M + H)^+$ 295.2. Found 295.3. ^{1}H NMR (500 MHz, DMSO-d_6) δ 9.04 (dd, J = 1.8, 1.0 Hz, 1H), 8.35−8.30 (m, 2H), 7.65 (dd, J = 9.4, 1.8 Hz, 1H), 7.56 (d, J = 9.4 Hz, 1H), 7.24 (t, J = 1.9 Hz, 1H), 7.13−7.04 (m, 2H), 6.54 (dt, J = 7.2, 2.0 Hz, 1H), 5.15 (s, 2H), 4.12 (dq, J = 13.6, 6.6 Hz, 1H), 1.19 (d, J = 6.7 Hz, 6H). ^{13}C NMR (151 MHz, DMSO-d_6) δ 163.3, 148.9, 146.4, 144.7, 134.0, 129.1, 127.9, 123.3, 120.0, 115.4, 113.8, 113.6, 111.2, 109.5, 41.2, 22.3.

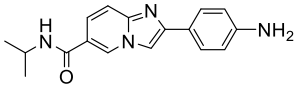

2-(4-Aminophenyl)-*N*-isopropylimidazo[1,2-*a*]pyridine-6-carboxamide. LRMS (+) calcd for $(M + H)^+$ 295.2. Found 295.3. ^{1}H NMR (600 MHz, DMSO-d_6) δ 8.98 (d, J = 1.7 Hz, 1H), 8.31 (d, J = 7.6 Hz, 1H), 8.21 (s, 1H), 7.67−7.62 (m, 2H), 7.61 (dd, J = 9.4, 1.8 Hz, 1H), 7.51 (d, J = 9.3 Hz, 1H), 6.64−6.58 (m, 2H), 5.28 (s, 2H), 4.11 (dq, J = 13.5, 6.7 Hz, 1H), 1.18 (d, J = 6.6 Hz, 6H). ^{13}C NMR (151 MHz, DMSO-d_6) δ 163.4, 148.9, 147.0, 144.7, 127.5, 126.8, 122.9, 121.16, 119.6, 114.9, 113.8, 107.5, 41.1, 22.4.

Representative Procedure for the SOF_4 Reaction.

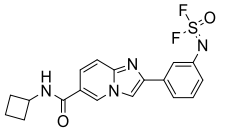

A 25 mL round-bottom flask equipped with a magnetic stir bar was charged with aniline (30.6 mg, 0.100 mmol) and DIPEA (38.8 mg, 52 μL, 0.300 mmol, 3.00 equiv). MeCN (1.0 mL) and DMF (1.0 mL) were added. Topped by a rubber septum, the flask was evacuated (solvent gently bubbling) and backfilled with thionyl tetrafluoride (O═SF_4). The mixture was stirred vigorously at room temperature for 30 min. The solution was then purified by reversed phase preparative high-performance liquid chromatography (HPLC) using a water/MeCN elution containing a 0.05 vol % TFA. The target compound (3-(6-(cyclobutylcarbamoyl)imidazo[1,2-*a*]-pyridin-2-yl)phenyl)sulfurimidoyl difluoride (compound **8**) was obtained as an off-white solid (TFA salt, 10.1 mg, 0.0200 mmol, 20%). LRMS (+) calcd for $(M + H)^+$ 390.1, found 390.1. ^{1}H NMR (600 MHz, DMSO-d_6) δ 9.22 (s, 1H), 8.95 (d, J = 7.4 Hz, 1H), 8.77 (s, 1H), 8.04 (dd, J = 9.4, 1.7 Hz, 1H), 7.91 (d, J = 9.4 Hz, 1H), 7.89−7.85 (m, 2H), 7.62 (t, J = 7.8 Hz, 1H), 7.35 (dd, J = 7.8, 2.0 Hz, 1H), 4.45 (q, J = 7.8 Hz, 1H), 2.30−2.21 (m, 2H), 2.10 (pd, J = 9.3, 3.0 Hz, 2H), 1.78−1.65 (m, 2H). ^{13}C NMR (151 MHz, DMSO-d_6) δ 162.1, 142.7, 140.0, 136.1, 131.0, 129.1, 127.8, 124.2, 122.5, 120.9, 116.5, 113.6, 112.0, 44.8, 30.0, 12.5. ^{19}F NMR (376 MHz, DMSO-d_6) δ 47.82, −74.61 (TFA). TLC R_f = 0.23 (10% MeOH in DCM).

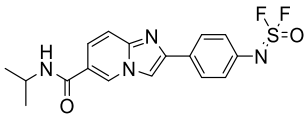

(4-(6-(Isopropylcarbamoyl)imidazo[1,2-*a*]pyridin-2-yl)-phenyl)sulfurimidoyl difluoride (compound **6**) (TFA salt, off-white solid, 5.5 mg). LRMS (+) calcd for $(M + H)^+$ 379.1. Found 379.1. ^{1}H NMR (600 MHz, DMSO-d_6) δ 9.14 (s, 1H), 8.63 (s, 1H), 8.47 (d, J = 7.6 Hz, 1H), 8.10−8.00 (m, 2H), 7.88 (d, J = 9.5 Hz, 1H), 7.74 (d, J = 9.4 Hz, 1H), 7.41 (d, J = 8.5 Hz, 2H), 4.13 (h, J = 6.7 Hz, 1H), 1.20 (d, J = 6.6 Hz, 6H). ^{13}C NMR (151 MHz, DMSO-d_6) δ 162.7, 158.2, 158.0, 135.4, 128.5, 127.5, 124.1, 116.8, 114.9, 114.5, 110.9, 41.3, 22.3. ^{19}F NMR (376 MHz, DMSO-d_6) δ 47.85, −74.37 (TFA).

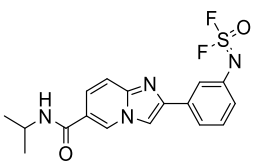

(3-(6-(Isopropylcarbamoyl)imidazo[1,2-*a*]pyridin-2-yl)-phenyl)sulfurimidoyl difluoride (compound **5**) (TFA salt, off-white solid, 21.8 mg, 0.0449 mmol, 44% isolated yield). LRMS (+) calcd for $(M + H)^+$ 379.1, found 379.1. ^{1}H NMR (600 MHz, DMSO-d_6) δ 9.17 (s, 1H), 8.70 (s, 1H), 8.51 (d, J = 7.7 Hz, 1H), 7.94 (dd, J = 9.4, 1.7 Hz, 1H), 7.91 (d, J = 8.0 Hz, 1H), 7.85 (t, J = 1.9 Hz, 1H), 7.79 (d, J = 9.3 Hz, 1H), 7.59 (t, J = 7.9 Hz, 1H), 7.31 (dd, J = 8.0, 1.3 Hz, 1H), 4.13 (dq, J = 13.5, 6.7 Hz, 1H), 1.20 (d, J = 6.6 Hz, 6H). ^{13}C NMR (151 MHz, DMSO-d_6) δ 162.5, 143.4, 140.8, 136.0, 132.8, 130.9, 128.7, 127.0, 124.1, 123.8, 122.1, 120.7, 114.3, 111.6, 41.4,

https://doi.org/10.1021/acscentsci.0c01550
ACS Cent. Sci. 2021, 7, 815−830

22.3. ^{19}F NMR (376 MHz, DMSO-d_6) δ 49.55, −74.35 (TFA). TLC R_f = 0.23 (10% methanol in DCM).

Representative Procedure for the Synthesis of Sulfamide.

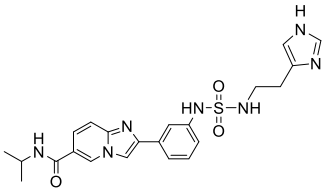

To a DMSO solution of (3-(6-(isopropylcarbamoyl)imidazo-[1,2-*a*]pyridin-2-yl)phenyl)sulfurimidoyl difluoride (∼7 mg, 18.5 μmol) was added histamine (24 mg, 132 μmol) in PBS, and the mixture was stirred overnight at 37 °C. To this solution was added histamine (12 mg, 66 μmol) in PBS (pH adjusted to 10 by NaOH), and the mixture was stirred overnight. The reaction mixture was directly purified on HPLC to give the target compound (compound **7**, 7 mg, 14.6 μmol, 79%). LRMS (+) calcd for (M + H)$^+$ 468.2. Found 468.5. ^{1}H NMR (600 MHz, DMSO-d_6) δ 9.86 (s, 1H), 9.11 (t, J = 1.3 Hz, 1H), 8.91 (d, J = 1.4 Hz, 1H), 8.46 (s, 1H), 8.40 (d, J = 7.7 Hz, 1H), 7.81−7.73 (m, 2H), 7.69 (t, J = 5.9 Hz, 1H), 7.65 (d, J = 9.4 Hz, 1H), 7.60 (dt, J = 7.7, 1.3 Hz, 1H), 7.37 (t, J = 7.9 Hz, 1H), 7.31 (d, J = 1.3 Hz, 1H), 7.18−7.12 (m, 1H), 4.17−4.07 (m, J = 6.7 Hz, 1H), 3.19 (q, J = 6.6 Hz, 2H), 2.80 (t, J = 6.8 Hz, 2H), 1.20 (d, J = 6.6 Hz, 6H). ^{13}C NMR (151 MHz, DMSO-d_6) δ 163.0, 144.4, 144.3, 139.3, 133.7, 133.5, 130.5, 129.5, 128.4, 124.6, 120.8, 120.3, 118.2, 116.3, 115.7, 115.2, 110.4, 41.3, 40.8, 24.4, 22.3.

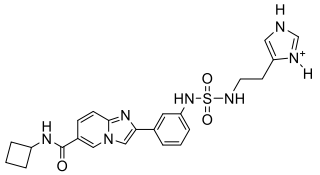

2-(3-((*N*-(2-(1*H*-Imidazol-4-yl)ethyl)sulfamoyl)amino)-phenyl)-*N*-cyclobutylimidazo[1,2-*a*]pyridine-6-carboxamide (TFA salt) (compound **9**). HRMS (+) calcd for (M + H)$^+$ 480.1818. Found 480.1813. ^{1}H NMR (600 MHz, DMSO-d_6) δ 9.86 (s, 1H), 9.12 (t, J = 1.4 Hz, 1H), 8.90 (d, J = 1.4 Hz, 1H), 8.79 (d, J = 7.4 Hz, 1H), 8.47 (s, 1H), 7.77 (p, J = 3.3 Hz, 2H), 7.74−7.65 (m, 2H), 7.60 (dt, J = 7.7, 1.3 Hz, 1H), 7.38 (d, J = 7.9 Hz, 1H), 7.31 (d, J = 1.3 Hz, 1H), 7.19−7.10 (m, 1H), 4.45 (h, J = 8.2 Hz, 1H), 3.19 (q, J = 6.7 Hz, 2H), 2.80 (t, J = 6.8 Hz, 2H), 2.25 (qt, J = 7.7, 2.8 Hz, 2H), 2.15−2.03 (m, 5H), 1.79−1.61 (m, 2H). ^{19}F NMR (376 MHz, DMSO-d_6) δ −74.43. ^{13}C NMR (151 MHz, DMSO-d_6) δ 162.7, 144.2, 143.9, 139.2, 133.6, 133.1, 130.3, 129.4, 128.4, 124.7, 120.5, 120.2, 118.2, 116.2, 115.6, 114.9, 110.4, 44.6, 40.7, 29.9, 24.3, 14.7.

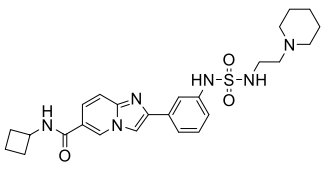

N-Cyclobutyl-2-(3-((*N*-(2-(piperidin-1-yl)ethyl)sulfamoyl)-amino)phenyl)imidazo[1,2-*a*]pyridine-6-carboxamide (compound **10**). HRMS (+) calcd for (M + H)$^+$ 497.2335. Found 497.2334. ^{1}H NMR (600 MHz, DMSO-d_6) δ 9.07 (dd, J = 1.8, 1.0 Hz, 1H), 8.73 (d, J = 7.4 Hz, 1H), 8.44 (d, J = 0.7 Hz, 1H), 8.28−8.19 (m, 2H), 7.82 (t, J = 1.9 Hz, 1H), 7.68 (dd, J = 9.5, 1.8 Hz, 1H), 7.63−7.57 (m, 2H), 7.36 (t, J = 7.9 Hz, 1H), 7.22 (s, 1H), 7.16 (ddd, J = 8.0, 2.3, 1.0 Hz, 1H), 4.46−4.42 (m, 1H), 2.96 (t, J = 7.0 Hz, 2H), 2.28 (dd, J = 11.3, 4.5 Hz, 2H), 2.27−2.16 (m, 6H), 2.13−2.10 (m, 2H), 1.75−1.65 (m, 2H), 1.37−1.34 (m, 4H), 1.30−1.21 (m, 2H). ^{13}C NMR (151 MHz, DMSO) δ 163.1, 145.5, 144.9, 139.4, 134.3, 129.3, 128.2, 123.5, 120.1, 119.9, 118.0, 115.7, 115.6, 110.2, 57.2, 53.9, 44.6, 40.1, 30.1, 25.4, 23.9, 14.8.

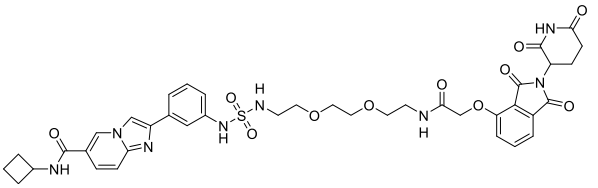

N-Cyclobutyl-2-(3-((*N*-(2-(2-(2-(2-((2-(2,6-dioxopiperidin-3-yl)-1,3-dioxoisoindolin-4-yl)oxy)acetamido)ethoxy)ethoxy)-ethyl)sulfamoyl)amino)phenyl)imidazo[1,2-*a*]pyridine-6-carboxamide (compound **4**). HRMS (+) calcd for (M + H)$^+$ 831.2772. Found 831.2776. ^{1}H NMR (600 MHz, Methanol-d_4) δ 9.11 (dd, J = 1.7, 1.0 Hz, 1H), 8.45 (d, J = 0.7 Hz, 1H), 8.07 (dd, J = 9.4, 1.7 Hz, 1H), 7.78 (dt, J = 9.4, 0.9 Hz, 1H), 7.78−7.69 (m, 2H), 7.53 (ddd, J = 7.7, 1.8, 1.0 Hz, 1H), 7.46−7.35 (m, 2H), 7.32 (dd, J = 8.5, 0.6 Hz, 1H), 7.25 (ddd, J = 8.1, 2.2, 1.0 Hz, 1H), 5.09 (dd, J = 12.8, 5.5 Hz, 1H), 4.65 (d, J = 1.6 Hz, 2H), 4.55−4.47 (m, 1H), 3.56 (s, 1H), 3.58−3.49 (m, 8H), 3.39 (dd, J = 5.9, 4.8 Hz, 2H), 3.36−3.30 (m, 1H), 3.21−3.14 (m, 2H), 2.86 (ddd, J = 17.4, 13.9, 5.4 Hz, 1H), 2.77−2.61 (m, 2H), 2.42−2.34 (m, 2H), 2.21−2.07 (m, 3H), 1.84 (s, 1H), 1.87−1.76 (m, 2H). ^{13}C NMR (151 MHz, methanol-d_4) δ 174.6, 171.5, 169.9, 168.2, 167.5, 164.7, 156.0, 144.0, 141.7, 141.2, 138.2, 134.7, 131.3, 130.7, 130.4, 130.4, 125.1, 122.0, 121.8, 121.4, 119.0, 117.8, 117.5, 114.1, 112.8, 71.3, 71.2, 70.8, 70.2, 69.0, 56.1, 43.9, 40.1, 31.24, 31.22, 29.5, 23.6, 16.1.

Safety Statement. No unexpected or unusually high safety hazards were encountered.

■ ASSOCIATED CONTENT

Supporting Information

The Supporting Information is available free of charge at https://pubs.acs.org/doi/10.1021/acscentsci.0c01550.

Characterization of SR-1114 in cells, characterization of the imidazopyridine series on-target and off-target effects, additional SR-0813 viability and growth assays, SR-0813 metabolic stability, and extended analysis of transcriptomics (Figures S1−S6) (PDF)

Expression proteomics (Table S1) (XLSX)

PSuFEx screen HTRF (Table S2) (XLSX)

SuFEx screening hits dose-response (Table S3) (XLSX)

SuFEx screen CETSA (Table S4) (PDF)

ENL and YEATS2 peptide array (Table S5) (XLSX)

BROMOscan data (Table S6) (XLSX)

KINOMEscan data (Table S7) (XLSX)

ENL ChIP-seq data (Table S8) (XLSX)

RNA-seq analysis (Table S9) (XLSX)

Gene sets (Table S10) (XLSX)

■ AUTHOR INFORMATION

Corresponding Author

Michael A. Erb − *Department of Chemistry, The Scripps Research Institute, La Jolla, California 92037, United States;*

https://doi.org/10.1021/acscentsci.0c01550
ACS Cent. Sci. 2021, 7, 815−830

orcid.org/0000-0001-9993-3481; Email: michaelerb@scripps.edu

Authors

Leopold Garnar-Wortzel − *Department of Chemistry, The Scripps Research Institute, La Jolla, California 92037, United States*

Timothy R. Bishop − *Department of Chemistry, The Scripps Research Institute, La Jolla, California 92037, United States*

Seiya Kitamura − *Department of Molecular Medicine and Department of Integrative Structural and Computational Biology, The Scripps Research Institute, La Jolla, California 92037, United States;* orcid.org/0000-0003-2453-849X

Natalia Milosevich − *Department of Chemistry, The Scripps Research Institute, La Jolla, California 92037, United States*

Joshua N. Asiaban − *Department of Chemistry, The Scripps Research Institute, La Jolla, California 92037, United States*

Xiaoyu Zhang − *Department of Chemistry, The Scripps Research Institute, La Jolla, California 92037, United States;* orcid.org/0000-0002-0951-9664

Qinheng Zheng − *Department of Chemistry, The Scripps Research Institute, La Jolla, California 92037, United States*

Emily Chen − *California Institute for Biomedical Research, The Scripps Research Institute, La Jolla, California 92037, United States*

Anissa R. Ramos − *Department of Chemistry, The Scripps Research Institute, La Jolla, California 92037, United States*

Christopher J. Ackerman − *California Institute for Biomedical Research, The Scripps Research Institute, La Jolla, California 92037, United States*

Eric N. Hampton − *California Institute for Biomedical Research, The Scripps Research Institute, La Jolla, California 92037, United States*

Arnab K. Chatterjee − *California Institute for Biomedical Research, The Scripps Research Institute, La Jolla, California 92037, United States*

Travis S. Young − *California Institute for Biomedical Research, The Scripps Research Institute, La Jolla, California 92037, United States*

Mitchell V. Hull − *California Institute for Biomedical Research, The Scripps Research Institute, La Jolla, California 92037, United States*

K. Barry Sharpless − *Department of Chemistry, The Scripps Research Institute, La Jolla, California 92037, United States*

Benjamin F. Cravatt − *Department of Chemistry, The Scripps Research Institute, La Jolla, California 92037, United States;* orcid.org/0000-0001-5330-3492

Dennis W. Wolan − *Department of Molecular Medicine and Department of Integrative Structural and Computational Biology, The Scripps Research Institute, La Jolla, California 92037, United States;* orcid.org/0000-0001-9879-8353

Complete contact information is available at: https://pubs.acs.org/10.1021/acscentsci.0c01550

Author Contributions

[▽]L.G.-W., T.R.B., and S.K. contributed equally.

Notes

The authors declare the following competing financial interest(s): S.K., A.K.C., D.W.W., and M.A.E are inventors on patent applications related to the molecules disclosed in this manuscript.

■ ACKNOWLEDGMENTS

We gratefully acknowledge L. L. Lairson for critically reading the manuscript; G. E. Winter for helpful discussions regarding the work; L. L. Lairson, P. G. Schultz, and I. A. Wilson for access to the instrumentation. We also thank P. G. Schultz and the Schultz laboratory for helpful discussions and technical support. Sequencing was performed by the Scripps Research Next Generation Sequencing Core (La Jolla). This work was supported by the National Institutes of Health (NIH) through an NIH Director's Early Independence Award (DP5-OD26380) to M.A.E., by the Leukemia and Lymphoma Society through a New Idea Award to M.A.E. and by the Ono Pharma Foundation to M.A.E. Research reported in this publication was also supported by the National Institute of General Medical Sciences of the National Institutes of Health under Award Number K99GM138758 (S.K.).

■ REFERENCES

(1) Kroon, E.; et al. Hoxa9 transforms primary bone marrow cells through specific collaboration with Meis1a but not Pbx1b. *EMBO J.* **1998**, *17*, 3714−3725.

(2) Lawrence, H.; et al. Frequent co-expression of the HOXA9 and MEIS1 homeobox genes in human myeloid leukemias. *Leukemia* **1999**, *13*, 1993−1999.

(3) Golub, T. R.; et al. Molecular Classification of Cancer: Class Discovery and Class Prediction by Gene Expression Monitoring. *Science* **1999**, *286*, 531−537.

(4) Afonja, O.; et al. MEIS1 and HOXA7 genes in human acute myeloid leukemia. *Leuk. Res.* **2000**, *24*, 849−855.

(5) Armstrong, S. A.; et al. MLL translocations specify a distinct gene expression profile that distinguishes a unique leukemia. *Nat. Genet.* **2002**, *30*, 41−47.

(6) Drabkin, H.; et al. Quantitative HOX expression in chromosomally defined subsets of acute myelogenous leukemia. *Leukemia* **2002**, *16*, 186−195.

(7) Alcalay, M.; et al. Acute myeloid leukemia bearing cytoplasmic nucleophosmin (NPMc+ AML) shows a distinct gene expression profile characterized by up-regulation of genes involved in stem-cell maintenance. *Blood* **2005**, *106*, 899−902.

(8) Argiropoulos, B.; Humphries, R. K. Hox genes in hematopoiesis and leukemogenesis. *Oncogene* **2007**, *26*, 6766−6776.

(9) The Cancer Genome Atlas Research Network. Genomic and epigenomic landscapes of adult de novo acute myeloid leukemia. *N. Engl. J. Med.* **2013**, *368*, 2059−2074.

(10) Erb, M. A.; et al. Transcription control by the ENL YEATS domain in acute leukaemia. *Nature* **2017**, *543*, 270−274.

(11) Wan, L.; et al. ENL links histone acetylation to oncogenic gene expression in acute myeloid leukaemia. *Nature* **2017**, *543*, 265−269.

(12) Krivtsov, A. V.; Armstrong, S. A. MLL translocations, histone modifications and leukaemia stem-cell development. *Nat. Rev. Cancer* **2007**, *7*, 823−833.

(13) Schulze, J. M.; Wang, A. Y.; Kobor, M. S. YEATS domain proteins: a diverse family with many links to chromatin modification and transcription. *Biochem. Cell Biol.* **2009**, *87*, 65−75.

(14) Hetzner, K.; García-Cuéllar, M.-P.; Büttner, C.; Slany, R. K. The interaction of ENL with PAF1 mitigates polycomb silencing and facilitates murine leukemogenesis. *Blood* **2018**, *131*, 662−673.

(15) Li, Y.; et al. Molecular Coupling of Histone Crotonylation and Active Transcription by AF9 YEATS Domain. *Mol. Cell* **2016**, *62*, 181−193.

(16) Nabet, B.; et al. The dTAG system for immediate and target-specific protein degradation. *Nat. Chem. Biol.* **2018**, *14*, 431−441.

(17) Filippakopoulos, P.; et al. Histone Recognition and Large-Scale Structural Analysis of the Human Bromodomain Family. *Cell* **2012**, *149*, 214−231.

(18) Wilson, B. G.; et al. Residual complexes containing SMARCA2 (BRM) underlie the oncogenic drive of SMARCA4 (BRG1) mutation. *Mol. Cell. Biol.* **2014**, *34*, 1136−1144.
(19) Hoffman, G. R.; et al. Functional epigenetics approach identifies BRM/SMARCA2 as a critical synthetic lethal target in BRG1-deficient cancers. *Proc. Natl. Acad. Sci. U. S. A.* **2014**, *111*, 3128−3133.
(20) Oike, T.; et al. A synthetic lethality-based strategy to treat cancers harboring a genetic deficiency in the chromatin remodeling factor BRG1. *Cancer Res.* **2013**, *73*, 5508−5518.
(21) Shi, J.; et al. Role of SWI/SNF in acute leukemia maintenance and enhancer-mediated Myc regulation. *Genes Dev.* **2013**, *27*, 2648−2662.
(22) Vangamudi, B.; et al. The SMARCA2/4 ATPase Domain Surpasses the Bromodomain as a Drug Target in SWI/SNF-Mutant Cancers: Insights from cDNA Rescue and PFI-3 Inhibitor Studies. *Cancer Res.* **2015**, *75*, 3865−3878.
(23) Papillon, J. P. N.; et al. Discovery of Orally Active Inhibitors of Brahma Homolog (BRM)/SMARCA2 ATPase Activity for the Treatment of Brahma Related Gene 1 (BRG1)/SMARCA4-Mutant Cancers. *J. Med. Chem.* **2018**, *61*, 10155−10172.
(24) Farnaby, W.; et al. BAF complex vulnerabilities in cancer demonstrated via structure-based PROTAC design. *Nat. Chem. Biol.* **2019**, *15*, 672−680.
(25) Schick, S.; et al. Acute BAF perturbation causes immediate changes in chromatin accessibility. *Nat. Genet.* **2021**, *53*, 269−278.
(26) Iurlaro, M.; et al. Mammalian SWI/SNF continuously restores local accessibility to chromatin. *Nat. Genet.* **2021**, *53*, 279−287.
(27) Gechijian, L. N.; et al. Functional TRIM24 degrader via conjugation of ineffectual bromodomain and VHL ligands. *Nat. Chem. Biol.* **2018**, *14*, 405−412.
(28) Christott, T.; et al. Discovery of a Selective Inhibitor for the YEATS Domains of ENL/AF9. *Slas Discov* **2019**, *24*, 133−141.
(29) Moustakim, M.; et al. Discovery of an MLLT1/3 YEATS Domain Chemical Probe. *Angew. Chem., Int. Ed.* **2018**, *57*, 16302−16307.
(30) Heidenreich, D.; et al. Structure-Based Approach toward Identification of Inhibitory Fragments for Eleven-Nineteen-Leukemia Protein (ENL). *J. Med. Chem.* **2018**, *61*, 10929−10934.
(31) Li, X.; et al. Structure-guided development of YEATS domain inhibitors by targeting π-π-π stacking. *Nat. Chem. Biol.* **2018**, *14*, 1140−1149.
(32) Ni, X.; et al. Structural Insights into Interaction Mechanisms of Alternative Piperazine-urea YEATS Domain Binders in MLLT1. *ACS Med. Chem. Lett.* **2019**, *10*, 1661−1666.
(33) Asiaban, J. N.; et al. Cell-Based Ligand Discovery for the ENL YEATS Domain. *ACS Chem. Biol.* **2020**, *15*, 895−903.
(34) Kitamura, S.; et al. Sulfur(VI) Fluoride Exchange (SuFEx)-Enabled High-Throughput Medicinal Chemistry. *J. Am. Chem. Soc.* **2020**, *142*, 10899−10904.
(35) Cromm, P. M.; Crews, C. M. Targeted Protein Degradation: from Chemical Biology to Drug Discovery. *Cell Chem. Biol.* **2017**, *24*, 1181−1190.
(36) Lu, G.; et al. The myeloma drug lenalidomide promotes the cereblon-dependent destruction of Ikaros proteins. *Science* **2014**, *343*, 305−309.
(37) Krönke, J.; et al. Lenalidomide causes selective degradation of IKZF1 and IKZF3 in multiple myeloma cells. *Science* **2014**, *343*, 301−305.
(38) Liu, F.; et al. Biocompatible SuFEx Click Chemistry: Thionyl Tetrafluoride (SOF4)-Derived Connective Hubs for Bioconjugation to DNA and Proteins. *Angew. Chem., Int. Ed.* **2019**, *58*, 8029−8033.
(39) Zhang, J.-H.; Chung, T. D. Y.; Oldenburg, K. R. A Simple Statistical Parameter for Use in Evaluation and Validation of High Throughput Screening Assays. *J. Biomol. Screening* **1999**, *4*, 67−73.
(40) Daigle, S. R.; et al. Selective Killing of Mixed Lineage Leukemia Cells by a Potent Small-Molecule DOT1L Inhibitor. *Cancer Cell* **2011**, *20*, 53−65.
(41) Kim, J.; et al. A Myc Network Accounts for Similarities between Embryonic Stem and Cancer Cell Transcription Programs. *Cell* **2010**, *143*, 313−324.
(42) Zuber, J.; et al. RNAi screen identifies Brd4 as a therapeutic target in acute myeloid leukaemia. *Nature* **2011**, *478*, 524−528.
(43) Zuber, J.; et al. An integrated approach to dissecting oncogene addiction implicates a Myb-coordinated self-renewal program as essential for leukemia maintenance. *Genes Dev.* **2011**, *25*, 1628−1640.
(44) Li, H.; et al. The EMT regulator ZEB2 is a novel dependency of human and murine acute myeloid leukemia. *Blood* **2017**, *129*, 497−508.
(45) Valk, P. J. M.; et al. Prognostically Useful Gene-Expression Profiles in Acute Myeloid Leukemia. *N. Engl. J. Med.* **2004**, *350*, 1617−1628.
(46) Raisner, R.; et al. Enhancer Activity Requires CBP/P300 Bromodomain-Dependent Histone H3K27 Acetylation. *Cell Rep.* **2018**, *24*, 1722−1729.
(47) Kaelin, W. G. Common pitfalls in preclinical cancer target validation. *Nat. Rev. Cancer* **2017**, *17*, 441−450.
(48) Winter, G. E.; et al. BET Bromodomain Proteins Function as Master Transcription Elongation Factors Independent of CDK9 Recruitment. *Mol. Cell* **2017**, *67*, 5−18.E19.
(49) Muhar, M.; et al. SLAM-seq defines direct gene-regulatory functions of the BRD4-MYC axis. *Science* **2018**, *360*, 800−805.
(50) Brand, M.; et al. Homolog-Selective Degradation as a Strategy to Probe the Function of CDK6 in AML. *Cell Chem. Biol.* **2019**, *26*, 300−306.E9.
(51) Vinogradova, E. V.; et al. An Activity-Guided Map of Electrophile-Cysteine Interactions in Primary Human T Cells. *Cell* **2020**, *182*, 1009−1026.E29.

https://doi.org/10.1021/acscentsci.0c01550
ACS Cent. Sci. 2021, 7, 815−830